Communication among Neurons. Quantitative Measures in Aging and Disease

Lisbeth Marner

This review has been accepted as a thesis together with 7 previously published papers by University of Copenhagen June 14th 2011 and defended on September 16th 2011.

Official opponents: Albert Gjedde, Ramin Parsey & Jørn Hounsgaard

Correspondence: Lisbeth Marner, PET and Cyclotron Unit, University Hospital of Copenhagen, Rigshospitalet, Blegdamsvej 9, 2100 Copenhagen, Denmark
E-mail: lisbeth@marner.dk

Dan Med J 2012;59(4): B4427

The thesis is based on the following studies:

I. Marner L, Nyengaard JR, Tang Y, Pakkenberg B. Marked Loss of Myelinated Nerve Fibers in the Human Brain with Age. *The Journal of Comparative Neurology* 462:144-152 (2003).
II. Marner L, Pakkenberg B. Total Length of Nerve Fibers in Prefrontal and Global White Matter of Chronic Schizophrenia. *Journal of Psychiatric Research* 37:539-547 (2003).
III. Jørgensen AM, Marner L, Pakkenberg, B.: No Change in Total Length of White Matter Fibers in Alzheimer's Disease. *Neuroscience* 157(4):878-883 (2008).
IV. Marner L, Gillings N, Comley RA, Baaré WFC, Rabiner EA, Wilson AA, Houle S, Hasselbalch SG, Svarer C, Gunn RN, Laruelle M, Knudsen GM. Kinetic Modeling of [^{11}C]SB207145 Binding to 5-HT$_4$ Receptors in the Human Brain *in vivo*. *Journal of Nuclear Medicine* 50(6):900-908 (2009).
V. Marner L, Gillings N, Madsen K, Erritzoe D, Baaré WFC, Svarer C, Hasselbalch SG, Knudsen GM. Brain Imaging of Serotonin 4 Receptors in Humans with [^{11}C]SB207145-PET. *Neuroimage* 50(3):855-861 (2010).
VI. Marner L, Knudsen GM, Haugbøl S, Holm S, Baaré W, Hasselbalch SG. Longitudinal Assessment of Cerebral 5-HT$_{2A}$ Receptors in Healthy Elderly Volunteers: An [^{18}F]-altanserin PET Study. *European Journal of Nuclear Medicine and Molecular Imaging* 36(2):287-293 (2009).
VII. Marner L, Frokjaer VG, Kalbitzer J, Lehel S, Madsen K, Baaré WFC, Knudsen GM, Hasselbalch SG. Loss of Serotonin 2A Receptors exceeds Loss of Serotonergic Projections in early Alzheimer's Disease: A combined [^{11}C]DASB-PET and [^{18}F]altanserin Study. *Neurobiology of Aging* 33(3):479-87 (2012).

IV, VI, and an earlier version of V without the occupancy part were included in my PhD thesis "Molecular Brain Imaging of the Serotonin System: Reproducibility and Evaluation of PET Radiotracers", April 2009, Faculty of Health Sciences, University of Copenhagen. The remaining studies have not been part of an academic degree.

SUMMARY

The communication among neurons is the prerequisite for the working brain. To understand the cellular, neurochemical, and structural basis of this communication, and the impacts of aging and disease on brain function, quantitative measures are necessary. This thesis evaluates several quantitative neurobiological methods with respect to possible bias and methodological issues.

Stereological methods are suited for the unbiased estimation of number, length, and volumes of components of the nervous system. Stereological estimates of the total length of myelinated nerve fibers were made in white matter of post mortem brains, and the impact of aging and diseases as Schizophrenia and Alzheimer's disease were evaluated. Although stereological methods are in principle unbiased, shrinkage artifacts are difficult to account for.

Positron emission tomography (PET) recordings, in conjunction with kinetic modeling, permit the quantitation of radioligand binding in brain. The novel serotonin 5-HT$_4$ antagonist [^{11}C]SB207145 was used as an example of the validation process for quantitative PET receptor imaging. Methods based on reference tissue as well as methods based on an arterial plasma input function were evaluated with respect to precision and accuracy. It was shown that [^{11}C]SB207145 binding had high sensitivity to occupancy by unlabeled ligand, necessitating high specific activity in the radiosynthesis to avoid bias. The established serotonin 5-HT$_{2A}$ ligand [^{18}F]altanersin was evaluated in a two-year follow-up study in elderly subjects. Application of partial volume correction of the PET data diminished the reliability of the measures, but allowed for the correct distinction between changes due to brain atrophy and receptor availability. Furthermore, a PET study of patients with Alzheimer's disease with the serotonin transporter ligand [^{11}C]DASB showed relatively preserved serotonergic projections, despite a marked decrease in 5-HT$_{2A}$ receptor binding. Possible confounders are considered and the relation to the prevailing β-amyloid hypothesis is discussed.

BACKGROUND

The human brain is a large, complex organ that is characterized by communication between its component cells, especially neurons. Other bodily organs as pancreas, gut, and adrenal glands excrete hormones to the blood stream and thereby communicate with cells far away. However, the intercellular communication of the brain has a far greater complexity, allowing for signaling between individual cells, or even between parts of cells. The number of neurons of a human brain outnumbers by far the transistors in the central processing unit (CPU) of any computer yet built. The CPU is digital, and thus limited to discrete binary states, with individual transistors serving as switches. However, neurons have an integrative function and spatial/temporal signaling far more complex than a simple switch. A typical mammalian neuron (pyramidal cell of the cerebral cortex) has hundreds of branchlike dendrites, each bearing numerous synapses with excitatory fibers that depolarize the dendritic membrane, and also inhibitory, hyperpolarizing synapses. All excitatory and inhibitory signals are integrated in a specialized extension of the soma called the axon hillock with the amplitude of each excitatory or inhibitory signal decreased exponentially with distance from the dendritic synapse giving rise to the signal. If a certain threshold (e.g. -70 mV) is reached in the axon hillock, voltage-gated ion-channels are activated and an action potential generated [1], i.e. the "transistor" is turned on transiently. Generally, the input to the neuron is through the synapses on the soma and dendrites, and the output is delivered by a fine extension known as the axon, typically arising from the axon hillock. This output, the action potential, is an electrical depolarization of the membrane propagating like a wave along the axon by means of transient opening of the voltage-gated ion-channels. The conduction velocity of this signal depends on the diameter of the axon and whether the axon is insulated with myelin. The myelin sheath consists of spiral, multilayered wrapping of the axon by membranes arising from nearby oligodendroglia cells. A major function of the sheath is to increase the conduction speed by restricting the flow of ionic current during the action potential to segments of the axon at the junction of two adjacent sheaths, known as the nodes of Ranvier. This results in saltatory conduction, which describes the jumping of impulses from node to node, normally proceeding in the direction away from the soma. Furthermore, the oligodendrocyte and its myelin sheaths are not simple insulators, but may be able to rapidly modulate the conduction speed so as to regulate and synchronize firing between neurons. This is accomplished by signaling to the oligodendrocytes by glutamate and potassium released by the neuron they ensheath [2]. The oligodendrocyte responds by regulating the myelination of its axons. Unmyelinated axons in mammals are generally less than 1 µm in diameter and conduct at less than 2.5 m/s, while myelinated axons are 1-20 µm in diameter and conduct at 3-120 m/s [1].

A wave of depolarization proceeds along the axon without attenuation, unlike dendritic signaling. At the end, or terminal, of the axon are specialized broadenings known as boutons, which are depolarized by the arrival of an action potential. The signal from the axon is next transmitted to recipient neurons across a gap known as the synapse, which is typically located on a dendrite of the neuron, although axosomatic, axoaxonal, and dendrodendritic synapses occur. The classical central nervous system synapse subserves neurochemical signaling, rather than a direct continuation of the electrical depolarization of the neuron of origin. At the synapse, the pre- and postsynaptic membranes come in close apposition, with the presynaptic bouton surrounding an elevation of the postsynaptic membrane, forming a so-called dendritic spine (figure 1).

The conduction across the synapse is usually one-way, with the exception of retrograde transmission by the endocannabinoid system. In general, arrival of the depolarization wave at the presynaptic terminal evokes exocytotic release of the contents of one or more vesicles. These vesicles contain high concentrations of the chemical signaling molecule, e.g. glutamate, gamma aminobutyric acid (GABA), dopamine, or serotonin, which, upon release, floods into the interstitial fluid, then diffuses across the gap or cleft separating the two neurons, and binds to receptors on the postsynaptic membrane. Transporters located on the presynaptic terminal facilitate the re-uptake of certain neurotransmitters, notably dopamine and serotonin.

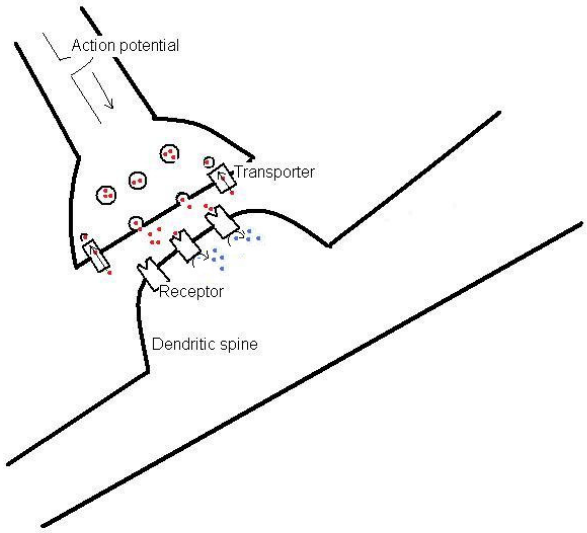

Figure 1
A synapse. At the arrival of the action potential, the neurotransmitter is released into the synaptic cleft separating the two neurons. The neurotransmitter binds to the receptors on the postsynaptic membrane which initiates an intracellular cascade of events modulating the membrane potential. In dopaminergic and serotonergic synapses, a transporter located presynaptically facilitate the re-uptake of the neurotransmitter for reuse.

By far the most excitatory neurons release the amino acid glutamate for signaling, while the main inhibitory neurotransmitter is another amino acid, GABA. The binding of neurotransmitter to ionotropic receptors opens ion channels within the receptor, permitting either an excitatory and depolarizing influx of cations, or an inhibitory and hyperpolarizing influx of chloride anions. Activation of metabotropic receptors initiates an intracellular cascade of events modulating the membrane potential, and its responsiveness to other signals, and sometimes with downstream effects on receptor trafficking, structural proteins or gene expression, which ultimately influence the strength of the synapse.

The basic neurobiology of neuronal communication thus resembles a CPU with a huge numbers of "transistors" but the complexity of each element is dramatically greater, due to the thousands of synapses on each neuron. Furthermore, the signaling by action potentials may not be simply digital "on" or "off" messages, but may entail frequency and pattern coding, analo-

gous to words of language [3]. As such, detailed modeling of the complexity of a single neuron might be a formidable task for high speed computers.

For comparison, a modern CPU contains a few billion transistors (10^9), while the human brain contains:

- 19-23 x10^9 neurons in neocortex [4].
- 29 x10^9 glia cells in neocortex [5].
- 164 x10^{12} synapses in neocortex [6].
- 28 x10^6 Purkinje cells in cerebellum [7].
- 109 x10^9 granule cells in cerebellum [7].

Brain serotonin (5-hydroxy-tryptophan, 5-HT) has been extensively studied due to the efficacy of serotonergic agents in the treatment of neuropsychiatric conditions including, major depressive disorder, obsessive compulsive disorder, and anxiety disorders. The serotonin receptors are divided into seven major classes, most of which have multiple subtypes, e.g. 5-HT_2 comprises three known subtypes, 5-HT_{2A}, 5-HT_{2B}, and 5-HT_{2C}. With the exception of 5-HT_3, which is a ligand-gated ion-channel, the 5-HT receptors are G-protein-coupled, with signal transduction mediated by either stimulation or inhibition of cAMP synthesis [8]. Most of the receptor subtypes are exclusively located postsynaptically, on neurons, astrocytes, and vascular elements while the 5-HT_1 receptors in the raphe nuclei are located presynaptically on the soma, dendrites, and axon terminals of serotonin neurons, and have an autoregulatory function.

The neurons of the raphe nuclei are the main source of serotonin in the brain giving rise to descending and ascending projections to every part of the brain. Serotonin has complex effects of neuroendocrine regulation and feeding, and is implicated in the regulation of aspects of cognition, mood, aggression, and perhaps personality traits [9;10].

The 5-HT_4 receptor has its' highest cerebral density in the basal ganglia and medium density in hippocampus [11]. Animal studies have found procognitive and memory enhancing effects of 5-HT_4 partial agonists [12-14] possibly mediated by a modulation of other neurotransmitter systems [15] such as the dopaminergic [16], GABAergic [17] and acetylcholinergic systems. Thus, 5-HT_4 agonists are shown to facilitate at least in part the release of the neurotransmitter acetylcholine in frontal cortex [18] and hippocampus [12].

Clinical trials (phase IIb) with a partial agonist are underway for the treatment of Alzheimer's disease (AD), based on the observation that 5-HT_4 receptor stimulation in a transgenic mouse model [19] increases the cerebral levels of the soluble amyloid precursor protein (sAPPα) that is believed to be neuroprotective and enhance memory consolidation [20]. This is achieved by diverting the cleavage pathway of the amyloid precursor protein, which thereby precludes the formation of the pathological and neurotoxic insoluble β-amyloid polypeptide [21], which is involved in Alzheimer's disease. Indeed, transgenic cortical cultures treated with a 5-HT4 partial agonist showed up to 95% lowering of the β-amyloid polypeptide concentration in a dose-dependent manner and exhibited higher neuronal survival [22]. In humans, the involvement of 5-HT_4 receptors in Alzheimer's disease has hitherto only been studied in post-mortem assays, which has given conflicting results [23;24].

AIMS

The aim of the present thesis was to evaluate quantitative neurobiological methods applied to measures of communication between neurons. The myelinated axons in the subcortical white matter and serotonin receptors and transporters were chosen as basic structures of neurotransmission, and these were evaluated with respect to aging and Alzheimer's disease.

- to evaluate the quantitative positron emission tomography (PET) methods, we aimed to validate a novel radioligand for quantitative PET imaging of 5-HT_4 receptors
- we aimed to estimate the total length of myelinated white matter fibers and evaluate the impact of sex, aging, schizophrenia, and Alzheimer's disease.
- to investigate the impact of atrophy, we aimed to measure the long-term stability of quantitative PET measures of 5-HT_{2A} receptors and the impact of partial volume effects.
- we aimed to exam if the known reduction in 5-HT_{2A} receptors in Alzheimer's disease could be attributed to a specific dysfunction of the serotonergic neurons and their projections.

QUANTITATIVE METHODS IN NEUROBIOLOGY

Why do we want to quantify? Why go through all the laborious details of measuring correctly, which a qualitative description may suffice? Lord Kelvin proclaimed in 1883 that "when you cannot measure it, when you cannot express it in numbers, your knowledge is of a meager and unsatisfactory kind". In the 16th century, scientists started to reject the qualitative science by Artistotle, as the quantitative method proved itself to be more correct. For example, Galileo showed by simple experiments that Aristotle's theory that heavier objects should fall faster than lighter objects is incorrect by simple measurements. The focus on quantification increased in the 19th century when von Humboldt traveled around the globe testing hypotheses and measuring everything from the number of head lice of natives to the height of mountains.

The standardization of units of measurements ensured objectivity and transfer of observations from site to site, which was important for the scientific revolution. Other sites must be able to confirm the measurements and use the findings as a basis for new experiments. For this purpose a standardization of units, parameters, methods, and nomenclature is generally important and in PET receptor research, the highly varying nomenclature was recently replaced by a consensus nomenclature developed by a large group of researchers in the field [25].

During the development of quantitative research, the error of measurements was measured and a language of accuracy was developed, which facilitated the reliable transfer of measurements from site to site, and ensured their trustworthiness. Thus, statistics is a crucial part of quantification, covering not only the measurement of error but also the limitations and potential biases of measuring and sampling. Especially when studying structures not visible to the human eye such as measures in neurobiology, the awareness of caveats and pitfalls is mandatory. The numerous corrections, delineations, rater-sensitive measures, chemical processing etc. can each bias the result, unless care is taken in each and every step of the analysis.

Stereology

Stereological methods are precise tools for obtaining quantitative information about 3D microscopic structures, based mainly on observations made in tissue sections. To avoid that the information obtained from 2D sections should be biased, some requirements must be fulfilled about the sections and the way they

are prepared [26]. The sampling technique is the basis of stereology and it is essential to ensure that the chosen sample is representative for a reference volume, i.e. the total volume of the tissue under study. Uniform random sampling is the most used method, because it efficiently ensures that all parts of the reference volume have the same probability of being sampled. Random sampling is ensured by the cast of dice or by consulting a random number table, as individuals will not choose randomly but will rather tend systematically to choose the larger volume, the area less affected by disease, or return to the same area, i.e. a person tend to choose number seven if asked to pick a number between one and ten.

If a brain is sliced into m slabs, systematic uniformly random sampling of 1/m of the slabs means that one of the first m slabs is taken at random and from then on every m^{th} slab is chosen from the ordered set of slabs, arranged in either their natural order or arranged in a smooth order [27]. The smooth order or the natural order which is often smooth in the context of studying biological structures, allows for sampling fewer slabs, since each slab resembles the one next to it. The uniform sampling diminishes the risk of sampling only that fraction of the organ containing a special structure, or only the largest slabs. The systematical random sampling of a tissue slab from a post mortem brain is provided as an example of these issues: The cerebral hemispheres are embedded in 6% agar and the right or left hemisphere is chosen systematically at random and cut into 5- to 7-mm-thick slabs starting at the frontal pole with a mean number of slabs per brain of 26±2.9. To sample approximately eight slabs per brain, the sampling fraction of slabs is 1:3 or 1:4, depending on the total number of slabs in each brain. A mean of 8.7±1.9 slabs per brain are sampled systematically by choosing one of the first three (or four) slabs randomly and then every third (or fourth) thereafter.

A principle in stereology is to reduce the possible factors influencing the estimated number. Densities are numbers per volume and will be dependent on both the number and the volume. For example, when the total number of particles in a structure is unchanged, shrinkage of the tissue can lead to an artificial increase in density. Thus, when reporting densities, care must be taken to ensure that the underlying assumption of comparable reference volumes is valid. By reporting total numbers in stereology instead of densities, the number of assumptions underlying the estimation is reduced.

The Cavalieri principle can be used to estimate the total volume of a structure, i.e. the reference volume. For example: The volume of white matter from one hemisphere was estimated using a counting grid with equidistantly placed points (area per point of 2.25 or 4.5 cm^2). The counting grid was placed at random (with closed eyes) on each slab and the points hitting the white matter were counted. The average slab thickness, t, was multiplied by the area per point, A_P, times the total number of points, P, from all slabs, to give the volume of white matter (V_{WM}) per hemisphere [26]: $V_{WM} = \sum P \cdot A_P \cdot t$. The total bilateral subcortical white matter volume was estimated by multiplying by two.

The measurement of number of microscopic particles in a reference volume using non-stereological methods is biased for a number of reasons. First, sectioning the tissue and counting the particles in 2D will lead to a volume bias, as larger particles will have a larger probability of being hit by a section. Second, larger particles of irregular form will have a different probability to be counted in the section as compared to small homogenous particles depending on the counting frame used. Correction for edge effects is not always sufficient.

The volume bias is overcome by using a physical or an optical disector. The physical disector consists of two thin sections in close proximity, with observation of the rule that only particles visible in one section and not the preceding one will be counted, each particle will only be counted once independently of size. The optical disector consists of a single thick section (typically 40 µm) and the counting frame is 3D as it uses the focal plane of the microscope for counting. A guard zone at the top and bottom is not included in the sampling interval to avoid bias from lost caps.

The unbiased counting frame is of major importance [28] (figure 2). This is designed to avoid bias due to size and shape of the particles. The counting frame is imposed a section of the tissue and particles inside the counting frame or touching the top and right green inclusion lines are included, whereas objects touching the bottom and left red lines are excluded. The design takes the higher probability of large objects to occur in a counting frame into account. The red exclusion lines are extended to avoid overestimation of snakelike particles. To understand fully the concept of the unbiased counting frame, one must imagine the entire section divided into counting frames lying side by side. Each particle can only be sampled in one of the counting frames and must be excluded if it appears in any other counting frame.

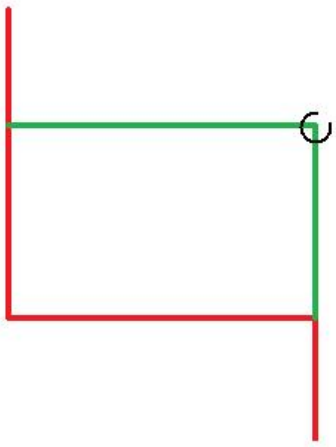

Figure 2
An unbiased counting frame, which is imposed on the tissue of interest. Only particles inside or touching the green inclusion lines are counted, while particles touching the red lines are excluded.

Diverse other quantitative stereological tools for the estimation of surface, connections, size of particles [26;27] have been developed but only the estimation of length will be described here: The total length of a structure may seem an unfamiliar measure. A simple cut through the reference volume, with counting the profiles per unit area, will only give information about the number of the structures passing more or less perpendicularly through this area. Other directions orientations of structures, or volume changes (due to preparation, disease, or age-changes) are important parameters, which are included in the total length estimation. To estimate the total length, systematical random sampling, randomly rotation of the tissue block, and the estimation of the reference volume are necessary.

In sections with a random orientation, the length density, L_V, i.e. the length of a structure per unit of volume, is estimated as [29]:

$$L_V = \frac{2 \cdot \text{Number of profile intersects}}{\text{Sampling area} \cdot (1 - \text{shrinkage})}$$

If the structures being measured are orientated in a uniformly random manner, i.e. with all possible orientations being represented by the same probability, each structure has exactly 50% possibility of being intersected by an arbitrary plane. Thus, the constant "2" in the formula correct for the structures not being intersected.

The total length in a reference volume (V_{REF}) is estimated by:

$$\text{Total length} = L_V \cdot V_{REF} \cdot$$

POSITRON EMISSION TOMOGRAPHY

Positron emission tomography (PET) enables the acquisition of quantitative 3D images of the distribution in the brain of molecules in nanomolar (10^{-9}) concentrations. For comparison millimolar (10^{-3}) concentrations are required for measurements using magnetic resonance imaging (MRI). Further in contrast to MRI, PET is in principle quantitative as the signal is linearly dependent on the concentration of the radioisotope per unit volume. It is possible to radiolabel the majority of biomolecules, while leaving them chemically indistinguishable from their unlabeled counterpart; in practice however, the brief physical halflife of the positron emitting isotopes (^{11}C, ^{13}N, ^{15}O, ^{18}F, ^{68}Ga, or ^{82}Rb) can preclude complex or low yield radiosynthesis. The positron emitted from the radionuclide annihilates with an electron, and two photons of energy 511 keV are emitted with an angle of nearly 180°. A PET scanner consists of detectors surrounding the subject (figure 3). The electronics of the individual detectors are linked so that the detections of two photons occurring within a certain time window (e.g. 10 ns) can be registered as a coincident event, most likely arising from the same annihilation. Each coincident event is assigned to a line of response joining the two relevant detectors. The distribution of the isotope can subsequently be reconstructed by estimating the original source distribution by either filtered back-projection (FBP) or by an iterative algorithm, e.g. ordered subset expectation maximization (OSEM).

Figure 3
The High Resolution Research Tomograph (HRRT) from Siemens at PET and Cyclotron Unit, Copenhagen University Hospital Rigshospitalet enables PET images with a theoretical resolution of a few millimeters.

Several sources of noise and bias are inherently present in the recordings and some are corrected for before and during the reconstruction of the PET image. Among these:

Dead-time. The recording (both the physical and electronic detection) of an event has a limited temporal resolution and at higher count rates, some events will not be detected due to occurrence in the refractory period of the detector after the preceding event, known as the dead-time. At count rates below a certain limit, dead-time effects can be corrected sufficiently for by modeling the losses of events before reconstruction.

Random coincidences. Some coincident events will be due to two random photons not originating from the same annihilation. This phenomenon is corrected for before the reconstruction using measurements of singles, i.e. photons detected with no co-photon detected within the time window.

Attenuation. Photons are lost during the passage from the site of emission through the body depending on the tissue (water, fat, bone, air) to the detectors. The attenuation by the tissues is corrected for within the reconstruction using a transmission scan with a gamma source measuring the loss of events in each line of response.

Scatter. During passage through the tissues, some photons will interact with electrons or nuclei and are scattered, i.e. change direction. This leads to a false line of response and especially in 3D recordings this is quantitatively important. Several methods for scatter correction in the reconstruction have been implemented.

To enable quantitative assessment of a molecule of interest using PET, a model is applied. The amount of tracer bound in the brain does not only reflect the number of molecules to which it binds to but depends also on the plasma concentration of tracer, the influx of tracer across the blood-brain-barrier, the affinity for binding the molecule of interest, the non-specific binding to other structures and tissue types etc. Several models for PET analysis are based on the dynamics of the tracer, and consideration of the temporal resolution of the PET relative to distribution kinetics is warranted. In dynamic recordings, the data is divided into a number of successive time frames, resulting in a series of images over time, thus constituting a 4D image. Individual PET frames can be complicated to assign anatomically; the usual practice is to align the temporally summed PET image to an MRI, in which anatomical regions can be defined. Then, regional time-activity curves can be extracted from the dynamic PET recording, and used for subsequent kinetic modeling.

When quantifying molecules of the brain, several requirements of the radioligand are of importance. In particular, a radioligand should:

- Bind selectively to the molecule with high affinity (nM range), and only to a minor degree to other receptor subtypes.
- Have a sufficiently high lipophilicity in order to cross the blood brain barrier.
- Have low non-specific binding, so as to obtain a high signal-to-noise ratio, i.e. the lipophilicity should not be too high.
- Have rather fast kinetics, such that equilibrium between association to and dissociation from the molecule of interest can occur within the time of endurable scan duration (and not more than six to eight half lives of the isotope).
- Be non-toxic, and not accumulate in body-parts especially sensitive to radioactivity, e.g. gonads.
- Be obtainable in injectable form via a reliable and fast radiosynthesis.

Additional requirements of a good tracer include low plasma protein binding, peripheral metabolism not resulting in lipophilic metabolites capable of entering the brain, and low substrate affinity for the brain efflux transporter, P-glycoprotein [30]. Furthermore, the existence of a reference region in the brain devoid of binding sites presents distinct advantages for widespread use of a radioligand.

Obtaining precise and unbiased quantitative measures of receptor concentrations in the human brain *in vivo* is a challenging task. The measured binding of the ligand to the receptor will depend not only on the receptor concentration (B_{max}), but also on the radioligand equilibrium dissociation constant (K_D) (inverse of affinity). The two parameters can be measured independently *in vivo* through serial injections of tracer at two or more concentrations, including a non-tracer dose resulting in partial receptor occupancy. Optimally, this is done in the same subject but a population-based estimation of K_D and B_{max} is possible too, which is intrinsically linked to the measurement of occupancy (see below).

Generally, PET examinations are carried out using a single tracer dose for estimation of the binding potential (*BP*), which is defined as the ratio of B_{max} to K_D. Binding potential quantifies the ratio of specific binding to a reference concentration at equilibrium; the specific type of binding potential is designated according to the chosen reference tissue concentration [25]:

- Free plasma concentration:

$$BP_F = \frac{B_{\max}}{K_D} = \frac{V_T - V_{ND}}{f_P}$$

- Total plasma concentration:

$$BP_P = f_P \frac{B_{\max}}{K_D} = V_T - V_{ND}$$

- Non-displaceable uptake:

$$BP_{ND} = f_{ND} \frac{B_{\max}}{K_D} = \frac{V_T - V_{ND}}{V_{ND}}$$

f_P being the free fraction (non-protein bound) of tracer in plasma and f_{ND} being the free fraction (non-bound) of tracer in (brain) tissue, V_T being the distribution volume in the tissue of interest, and V_{ND} being the distribution volume in a reference region with only non-displaceable binding. The term distribution volume originates from clinical pharmacology and refers in the context of PET to the volume of plasma needed to account for the radioligand in a brain region where the tracer is evenly distributed between brain and plasma. Thus, if the concentration at equilibrium is five times the concentration in plasma, then V_T=5, indicated that five volumes of plasma would be needed to contain the same amount of radioligand as in a volume of brain. It must be noted that V_T is a sum of the distribution volumes of free ligand in tissue water, specifically bound ligand, and nonspecifically bound ligand.

To obtain estimates of distribution volumes, V_T or V_{ND}, compartmental analysis can be used, or alternatively, PET recordings can be made at equilibrium, which is obtained by constant infusion of the tracer to induce steady state conditions. In this circumstance, the distribution volumes are calculated directly, knowing only the plasma and brain concentrations, such that BP_P is easily achieved: $BP_P = V_T - V_{ND} = \frac{C_T - C_{ND}}{C_P}$

where C_P is the plasma concentration of unmetabolized radiotracer, C_T is the radioactivity concentration in the target region, and C_{ND} the concentration in the reference region. As noted above, similar estimates can be obtained through application of a tracer kinetic model, which requires a dynamic recording (4D) with serial arterial blood sampling and measurements of plasma radioactivity concentration and tracer metabolites.

In general, the kinetic models for receptors ligands are simple extensions of a cerebral blood flow model, with additional terms for the binding of radioligand to receptors, and dissociation, for the case of reversible binding ligands. Influx across the blood-brain-barrier, except when mediated by a carrier is not saturable, and binding to receptors is not saturated at tracer doses, as defined by <5-10% of receptors occupancy. As such, ligand binding is only dependent on the unbound concentration of the tracer in brain tissue (which is itself determined by the permeability of the blood brain barrier and blood flow). In the special case of tracers, which are substrates for the P-glycoprotein efflux transporter, self-competition or inhibition by other substrates can enhance the net tracer uptake in brain.

The general kinetic model contains one, two or three tissue compartments (1TC, 2TC and 3TC), as well as plasma. Traditionally, the first tissue compartment is the free ligand, the second the specific binding, and the third is composed of the non-specific binding (figure 4).

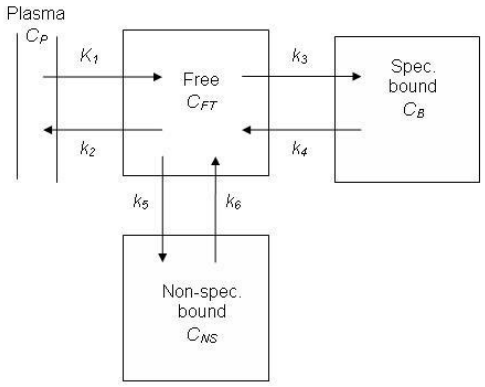

Figure 4
The possible compartment s in a kinetic model. The rate constants K_1, k_2, k_3, k_4, k_5 and k_6 describe the flux of tracer between plasma and the three tissue compartments (free, specifically bound and non-specifically bound). In most applications, a maximum of only two tissue compartments can be distinguished kinetically.

The unidirectional blood-brain clearance (K_1) has units of cerebral blood flow (mL cm^{-3} min^{-1}), and the other defined processes (k_2, k_3, k_4, k_5, k_6) are fractional rate constants (min^{-1}). In most cases it is not possible, given the noise properties of PET recordings, to separately determine the masses occupying the three tissue compartments. Therefore, the free and non-specific compartments are often regarded as a single compartment, and only four rate constants are used to describe the biological system. Thus, the number of compartments should not be viewed strictly in biological terms, since the number of rate constants to be measured depends on what can be separated kinetically. Consequently, the reference tissue may actually have two tissue compartments (free and non-specific compartments), while the tracer kinetics in the high binding tissue may be best described with only one.

The distribution volume at equilibrium can be estimated from the rate constants obtained dynamically [31] depending on the number of tissue compartments:

1TC model: $V_T = \frac{K_1}{k_2}$,

2TC model: $V_T = \frac{K_1}{k_2}$, and

3TC model: $V_T = \left(\frac{K_1}{k_2}\right)\left(1+\frac{k_3}{k_4}+\frac{k_5}{k_6}\right)$.

To obtain the rate constants, we need to know the input to the brain, i.e. the tracer concentration in arterial blood as a function of time, and the output, i.e. the tissue concentrations averaged for all compartments, also as a function of time. Thus, the radiotracer plasma time-activity curve (corrected for radiolabeled metabolites of the tracer) defines the input to the brain, and the time-activity curves derived from the dynamic PET scan is the output.

If a 2TC model is assumed, then the changes in concentrations of free tracer, C_{FT} (which includes the non-specifically bound ligand) and specifically bound tracer C_S can be described by the differential equations (differentiated with respect to time, t):

$$\frac{dC_{FT}}{dt} = K_1 C_P - k_2 C_{FT} - k_3 C_{FT} + k_4 C_S$$

$$\frac{dC_S}{dt} = k_3 C_{FT} - k_4 C_S$$

The solution can be written as the arterial input function convoluted to a sum of exponentials [31]. Thus, when knowing the plasma input curve, the regional rate constants are fitted to the regional PET time-activity curves, for estimation of the distribution volumes and binding potentials defined in the model. In general, the estimation of individual rate constants knwn as microparameters, is not as robust as the estimation of macroparameters, such as V_T. Modeling the V_T using 1TC or 2TC models and the metabolite corrected arterial plasma input is regarded as the gold standard.

Reference Tissue Models

Measuring the plasma input curve to the brain requires invasive arterial cannulation and labor-intensive measuring of radiolabeled metabolites, which often introduces noise into the measurements. If a true reference tissue exists, demonstrably devoid of specific binding, and with similar non-specific binding as the rest of the brain, use of a non-invasive reference tissue model becomes feasible [32]. The reference tissue models are very useful, as they obviate the need for labor-intensive blood sampling and metabolite analyses. Furthermore, the lower levels of noise in the estimated parameters are more conductive for the detection of pharmacologically-evoked changes in binding potentials to be more readily detected. However, the end point, BPND, is relative to in non-displaceable binding, and changes in specific binding cannot be separated from changes in non-displaceable binding [33]. Thus, the risk of biased estimates is higher with reference tissue models than with arterial input models, which allow for estimation of BP_P or BP_F or at least allow for checking the assumption of no differences in V_{ND} between groups. On the other hand, BP_P of BP_F assume that the total or free plasma concentration is available for entry into brain, and estimates may be biased from P-glycoprotein effects that would cancel out in the estimation of BP_{ND}, assuming that P-glycoprotein is homogenously distributed.

The widely-used simplified reference tissue model (SRTM) [34] allows for fitting the region of interest with the reference region serving as an indirect input function, yielding robust estimates for BP_{ND}, k_2 (the washout rate constant) and $R_1 = K_1/K_1'$ (relative delivery, K_1' is the unidirectional blood brain clearance for the reference tissue). The assumptions of the model include:

- that the non-displaceable distribution volume (V_{ND}) in the region of interest and in the reference tissue being the same, i.e. $K_1'/k_2' = K_1/k_2$.
- that tracer kinetics in the target region (as well as the reference tissue) are such that it is difficult to distinguish between free and specific compartments, i.e. can be fitted satisfactorily with a 1TC model, without distinct k_3 and k_4 terms.

The SRTM is expressed as:

$$C_T(t) = R_1 C_{ND}(t) + \left(k_2 - R_1 \frac{k_2}{1+BP_{ND}}\right) C_{ND}(t) \otimes e^{\frac{-k_2 t}{1+BP_{ND}}}$$

where t is time, and $\otimes$ denotes convolution. It has been shown for the case of [^{11}C]raclopride that, even when the second of the above assumptions is not met, i.e. kinetics in the target tissue is actually best described by a 2TC model, the SRTM remains sensitive to changes in binding potential in human brain [34]. However, when the assumption of 1TC kinetics in the reference tissue is not met, a bias appears especially in regions with high binding [33].

Other reference models include a Logan plot [35] using the reference tissue as input instead of metabolite corrected plasma input [36], derivations of the Logan plot, e.g. multilinear reference tissue model (MRTM and MRTM2) [37], and other methods using integrals to reduce the sensitivity to noise [38]. The Logan plot is a linearization of the tissue concentrations integrated to circulation time T:

$$\frac{\int_0^T C_T(t)dt}{C_T(T)} = (1+BP_{ND}) \cdot \frac{\int_0^T C_{ND}(t)dt + \frac{C_{ND}(T)}{k_2'}}{C_T(T)} + \beta$$

where C_T is the total concentration in the tissue of interest, C_{ND} the concentration in the reference tissue, k_2' is the washout rate constant for the reference tissue, T is the time point, and β the intercept. If tracer kinetics are sufficiently fast, at some time t*, the plot becomes linear and the slope is $1+BP_{ND}$. The Logan plot presents a computational advantage in its fast linear calculation and lacks the assumptions of 1TC or 2TC kinetics. Its limitations are derived from the dependence on choosing a proper t^*, and a noise-induced bias due to $C_T(T)$ on both sides of the equation. The latter has been overcome by the derivations by Ichise, of the MRTM and the MRTM2 with fixed k_2' [37]. Especially when generating parametric images, i.e. images of binding potentials, with calculations for each voxel of the PET image, fast calculations by linearizations are an advantage. Although nonlinear, the SRTM can be used for rapid calculation of parametric images by selecting functions from an overcomplete dictionary of kinetic basic functions [39] enabling fast calculations.

The novel radioligand [^{11}C]SB207145 was introduced for PET imaging of 5-HT_4 receptors in the living brain. It was shown in pigs to enter the brain readily and distribute in a manner consistent with the known 5-HT_4 densities (striatum>thalamus>cortical regions>cerebellum) [40]. In the minipig, [^{11}C]SB207145 time activity curves are described equally well by 1TC and 2TC kinetics in all brain regions. The simplified reference tissue model with fixed k_2' [41] provided stable and precise estimates of the BP_{ND}, which were highly correlated to binding in vitro, as measured in the same pigs' brains [42].

In **study IV** of the thesis, the tracer quantification was investigated with 1TC and 2TC models, and also SRTM, in test-retest and blocking PET experiments. The several models were assessed in

terms of their goodness-of-fit, and reproducibility and reliability on test-retest data.

Six healthy subjects were included in the test-retest part of **study IV** (age-range 21-44 years, 3 men) that was performed at Copenhagen University Hospital, Rigshospitalet, Copenhagen, Denmark. Subjects received in the morning and again in the afternoon a bolus injection of [^{11}C]SB207145, and a two-hour dynamic emission scan was acquired with a GE-Advance scanner operating in 3D-acquisition mode, with an approximate in-plane resolution of 6 mm. The emssion frames were reconstructed using filtered back projection (6 mm Hann filter and 8.5 mm axial ramp filer) and corrected for randoms, deadtime, scatter, and attenuation [43]. Arterial blood samples for measurement of the radioactivity concentration were drawn at 5-10 s intervals during the first two min and subsequently at the mid frame times. In addition, seven samples were acquired for plasma metabolite measurements.

The PET frames were aligned to correct for motion artifacts and an early frame (15-20 min) with cerebral blood flow-like tracer distribution was aligned to the individual's MRI. The MRI was segmented into gray and white matter by means of the Statistical Parametric Mapping (SPM2) program and a total of 19 regions in both hemispheres were automatically delineated [44] on each subject's MRI in a user-independent fashion. The regions of interest were applied to the dynamic PET data and decay-corrected time-activity curves were derived (figure 5). The parent arterial plasma input function was calculated as the total measured plasma activity multiplied by the fitted parent fraction and constrained to be equal to a sum of exponentials following the peak (figure 6).

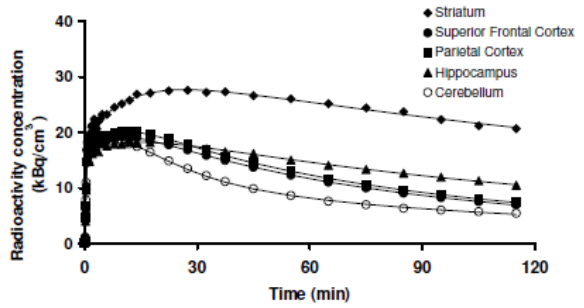

Figure 5
Regional time-activity curves in the brain of a 36 year old female of 69 kg weight after injection of 512 MBq [11C]SB207145. The striatum shows the highest and latest peak and the slowest washout due to the high density of receptors while superior frontal and parietal cortices show a faster washout. Cerebellum, which is devoid of specific binding has the fastest washout. The fittings with 2-TC modeling are shown (from **study IV**).

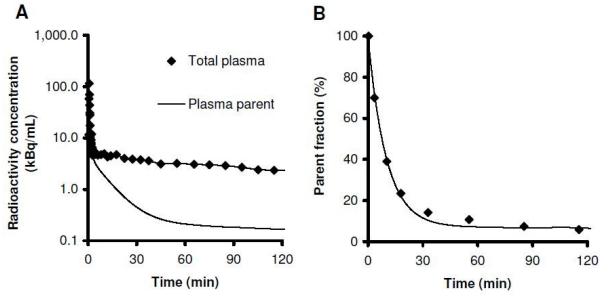

Figure 6
A: The total radioactivity concentration in plasma and the metabolite corrected plasma radioactivity in the same subject as figure 5. B. Metabolite measurements of a representative subject. The fitting is a constrained bi-exponential function [45] (from **study IV**).

Kinetic Modeling

Modeling was performed using in-house software at GSK implemented within Matlab applying the basis function implementation [46] for SRTM. Three kinetic models were investigated using the test-retest data (1TC, 2TC models and SRTM) and were compared using the Akaike Information Criteria for goodness-of-fit, as well as test-retest reproducibility and reliability:

$$\Delta\% = \frac{2 \cdot (retest\_value - test\_value)}{test\_value + retest\_value} \cdot 100\%$$

the mean of Δ% across subjects is a measure of systematic differences (bias) and the standard deviation of Δ% is referred to as the average test-retest difference, which characterizes the reproducibility [47].

Reliability was assessed using the intraclass correlation coefficient (*ICC*), determined as:

$$ICC = \frac{MSS_{Between} - MSS_{Within}}{MSS_{Between} + MSS_{Within}}$$

$MSS_{Between}$ and MSS_{Within} are the mean sum of squares between and within subjects. An *ICC* score of –1 denotes no reliability and +1 denotes maximum reliability.

The kinetics of the radioligand are reversible and well described by a 2TC plasma input model (table 1 and figure 7).

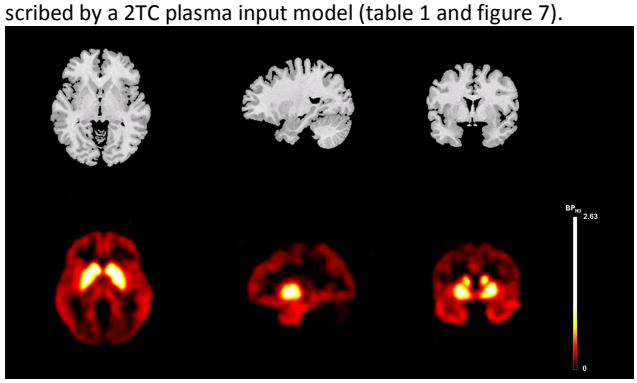

Figure 7
Cerebral 5-HT4 receptor distribution in a healthy 36-years old female as measured with [11C]SB207145-PET (bottom) and MRI from the same subject (top). The parametric BPND image was calculated using MRTM2 [37] (from study V).

In addition, the SRTM with cerebellum input successfully quantified the binding of the radiotracer, although we observed a slight overestimation of BP_{ND} in the cortical regions and an underestimation of 20-43% in striatum when using the SRTM as compared to 2TC modeling (figure 8).

Table 1.

Parameter estimation for kinetic modeling with [^{11}C]SB207145.

	Regions	K_1 (mL cm^{-3} min^{-1})	k_2 (min^{-1})	k_3 (min^{-1})	k_4 (min^{-1})	V_T (mL/cm^3)	BP_{ND}	BP_P (mL/cm^3)	Akaike Inf. Crite-ria	Relative diff BP_{ND} (%)	Ave-rage diff. BP_{ND} (%)	*ICC* BP_{ND}	Relative diff. BP_P (%)	Ave-rage diff. BP_P (%)	*ICC* BP_P
1-TC model	Cerebellum	0.19±0.07	0.023±0.003	-	-	7.86±2.23	-	-	586±20	-	-	-	-	-	-
	Parietal ctx	0.19±0.07	0.016±0.003	-	-	11.8±3.26	0.51±0.10	3.97±1.22	542±26	7.50	13.2	0.82	11.6*	10.7	0.88
	Sup. fr. ctx	0.19±0.07	0.016±0.003	-	-	11.3±3.17	0.43±0.10	3.39±1.16	541±23	8.08	12.5	0.87	12.2*	9.70	0.89
	Hippocampus	0.17±0.06	0.010±0.002	-	-	16.2±4.59	1.07±0.21	8.38±2.63	569±13	6.27	13.0	0.80	10.4*	7.53	0.91
	Striatum	0.23±0.08	0.006±0.002	-	-	40.4±11.7	4.20±0.93	32.5±10.1	536±27	11.4**	8.2	0.84	15.5*	8.69	0.80
2-TC model	Cerebellum	0.24±0.08	0.056±0.009	0.021±0.01	0.018±0.003	9.50±2.58	-	-	510±28	-	-	-	-	-	-
	Parietal ctx	0.23±0.08	0.054±0.019	0.099±0.08	0.050±0.023	12.3±3.42	0.30±0.08	2.83±1.02	506±30	11.9	13.6	0.80	13.8*	10.7	0.87
	Sup. fr. ctx	0.22±0.08	0.057±0.021	0.108±0.08	0.050±0.023	11.7±3.32	0.23±0.08	2.22±0.95	504±26	17.7	19.4	0.79	19.7*	11.8	0.84
	Hippocampus	0.23±0.07	0.110±0.032	0.178±0.06	0.026±0.008	17.3±5.01	0.82±0.19	7.81±2.73	517±21	10.9	12.9	0.82	12.8*	5.95	0.90
	Striatum	0.27±0.09	0.066±0.032	0.364±0.13	0.060±0.063	41.4±12.0	3.38±0.72	31.9±10.0	519±31	13.9*	7.9	0.68	15.8**	7.82	0.81
SRTM	Cerebellum	-	0.016±0.012	-	-	-	-	-	-	-	-	-	-	-	-
	Parietal ctx	-	0.069±0.011	-	-	-	0.36±0.06	-	449±25	5.73	13.6	0.77	-	-	-
	Sup. fr. ctx	-	0.067±0.008	-	-	-	0.30±0.07	-	467±20	6.60	12.6	0.84	-	-	-
	Hippocampus	-	0.037±0.005	-	-	-	0.70±0.13	-	517±14	4.00	9.92	0.88	-	-	-
	Striatum	-	0.054±0.004	-	-	-	2.21±0.21	-	496±28	3.74	6.06	0.76	-	-	-

K_1, k_2, k_3, and k_4 are rate constants. VT is the total volume of distribution. $BP_{ND}=V_T/V_{ND}-1$ is the binding potential relative to non-displaceable binding and $BP_P=V_T-V_{ND}$ relative to plasma. The (minimum) Akaike Information Criterion indicates a more statistically appropriate model. The relative test-retest differences is $\Delta\%=2*(\text{scan2-scan1})/(\text{scan1+scan2})*100\%$. The average test-retest difference is the standard deviation (SD) of Δ %. The intraclass correlation coefficient (ICC) indicates the reliability. * $p<0.05$, ** $p<0.01$.

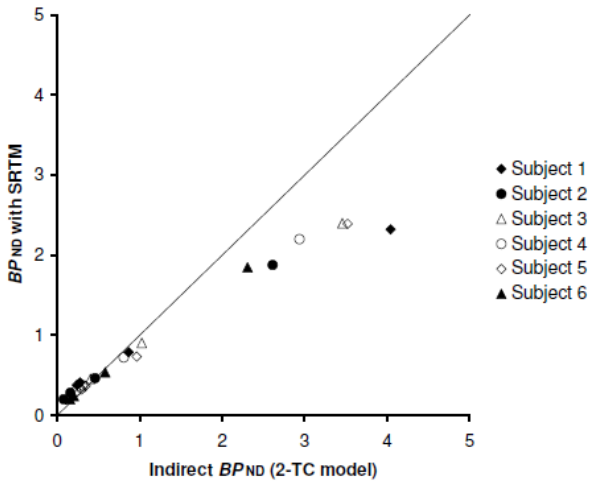

Figure 8
BP_{ND} estimated with the SRTM compared to BP_{ND} determined indirectly from V_T (2-TC model with arterial input). The graph shows bias in areas of high binding with SRTM (on average 30%, range 20-43%). The solid line is the line of identity (from **study IV**).

The bias is most likely a result of violations of SRTM assumptions that require 1TC kinetics in cerebellum [33], although noisy measurements at late time points of the input function can lead to inflated BP_{ND}'s with the 2TC model. The SRTM yielded low test-retest differences (6-10% in moderate- to high-binding regions and 12-14% in low-binding regions) and high reliability (*ICC*: 0.76-0.88). The low-binding cortical regions have BP_{ND} in the range of only 0.3-0.4. Nonetheless, the observed reproducibility and reliability support the use of cortical binding potentials in future clinical studies.

Validation of a Reference Region

A reference region is often used to correct for non-specific binding of tracer. To obtain measures of V_{ND} (or C_{ND}), a receptor-devoid reference region must be present and the non-specific binding should be homogenous throughout the brain. The validation of a reference region requires a blocking study, which is included in **study IV**.

Two healthy men (aged 37 and 29) were included in the blocking study that was performed at the Vivian M. Rakoff PET Centre, Centre for Addiction and Mental Health, Toronto, Canada. [^{11}C]SB207145 PET scans were acquired pre-and post oral administration of the selective 5-HT_4 inverse agonist, Piboserod (SB207266) [48]. The blocking reduced time activity curves and resultant binding outcome measures in all regions studied, except in the cerebellum, where distribution volumes were not changed (figure 9 and 10).

These data support the use of the cerebellum as a reference region and the assumption of homogeneous non-specific binding throughout the brain. In addition, they confirm the selectivity of the specific signal for the 5-HT_4 receptor.

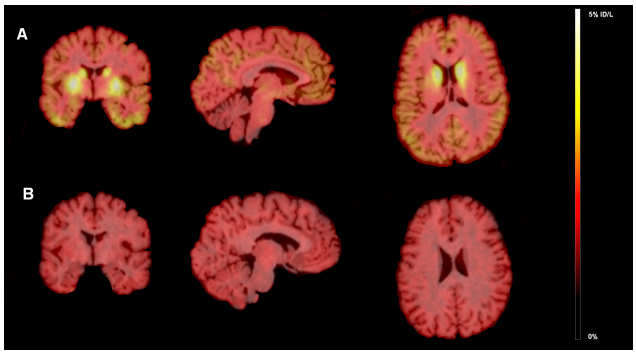

Figure 9
Baseline (A) and a blocked (B) [11C]SB207145 images (male, 29 years) before and after oral administration of the structurally dissimilar inverse agonist Piboserod (SB207266; 150 mg p.o.). The mean images from 30 to 120 min after injection are normalized to injected dose (ID) to obtain a normalized uptake value. The chosen orthogonal sections pass through striatum (from **study IV**).

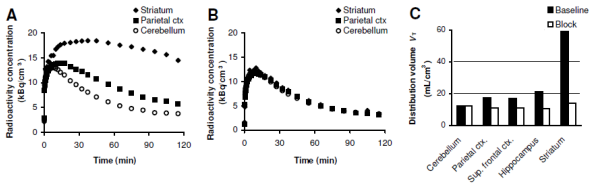

Figure 10
Time activity curves for the baseline (A) and the blocked (B) scans (male, 29 years). After administration of Piboserod (SB207266), the [^{11}C]SB207145 distribution volumes (C) are reduced to that of cerebellum at baseline (n=2) (from **study IV**).

Occupancy

When performing a PET experiment, the specific activity (the radioactivity concentration per mass of tracer), should be sufficiently high to enable tracer concentrations resulting in less than 5-10 % of the receptors being bound to tracer. If a larger mass of tracer is injected, a considerable proportion of the receptors will be occupied with non-labeled (cold) tracer. Measurements of binding will then be biased, as the concentration of available receptors, B_{avail}, is discernibly lower than B_{max}. Furthermore, accidental administration of significant masses of some agonists has in the past made patients ill by exerting pharmacological effects. Therefore, radioligands have generally been used at a tracer dose, i.e. never occupying more than 5-10% of the receptors, except in PET studies specifically designed to measure the absolute abundance of receptors.

When performing the initial experiments on the first 16 subjects with the new tracer [^{11}C]SB207145, too low specific activity resulted in lack of tracer doses for some of the subjects, in whom the occupancy was as high as 28% (study V). However, the range in amount of injected unlabelled ligand enabled the estimation of a population-based B_{max} and K_D *in vivo* by fitting the following relationship (figure 11):

$$B = \frac{B_{max} \cdot F}{F + K_D} \Leftrightarrow \frac{B}{F} = \frac{B_{max}}{F + K_D}$$

where *B* and *F* are the concentrations of bound and free ligand. For an unbiased estimate of B/F, the BP_{ND} was used, while *F* was estimated as the mean radioactive concentration in cerebellum, C_{ND}, divided by the specific activity prevailing at the later time points of the time activity curve (40-110 min). In that time interval, the ratio between cerebellar and striatal radioactivity concentration was relatively stable, resembling steady-state. To reduce noise in the estimation of B_{max}, K_D was fixed to the value obtained in striatum, given that earlier *in vitro* findings have suggested a uniform K_D for this [^{11}C]SB207145 throughout the brain [42].

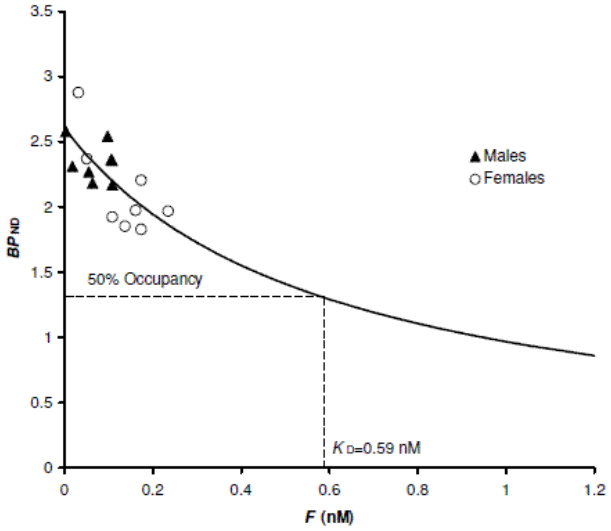

Figure 11
Striatal BP_{ND} as a function of the concentration of free SB207145 in cerebellum (*F*). The fitting of $BP_{ND}=B_{max} / (F+K_D)$ is indicated and K_D (the concentration of *F* that leads to 50% binding) is 0.59 nM.

The occupancy (*O*) was estimated for each individual as:

$$O = \frac{B}{B_{max}} = \frac{F}{F + K_D}$$

and the BP_{ND} was subsequently individually corrected by dividing by 1-*O*. For repeated scans, residual ligand from any first scan, $F_{Baseline}$, in the second scan, *F* was estimated as:

$$F = \frac{C_{ND}(80-120\,\text{min})}{SpecificActivity} + F_{Baseline}e^{-wo \cdot t}$$

where *wo* is the wash-out from cerebellum (mono-exponential function fitted to the last 60 min) and *t* the time elapsed since baseline scan; on average 18±7.3% of *F* was residual ligand from first scan.

The effective dose for occupying 50% of the receptors, ED_{50} [49], was estimated by plotting the measured occupancy as a function of the injected dose (*D*) divided by body mass (µg/kg) and fitting the data to the saturation function $O = D / (D + ED_{50})$, ED_{50} = 0.33 µg/kg to the data. By this means, we found that to ensure tracer doses (occupancy < 5%), the mass should be kept below 0.017 µg/kg (1.2 µg for a 70 kg subject) per PET examination.

Populations-based B_{max} estimates for the caudate nucleus, lentiform nucleus, temporal cortex, hippocampus, amygdala and frontal cortex were estimated with the fixed K_D (**study V**) and compared to literature values for B_{max} from a post mortem homogenate binding study in humans [50]. A significant correlation (Spearman's r = 0.86, p = 0.04) to B_{max} *in vivo* was found (figure 12).

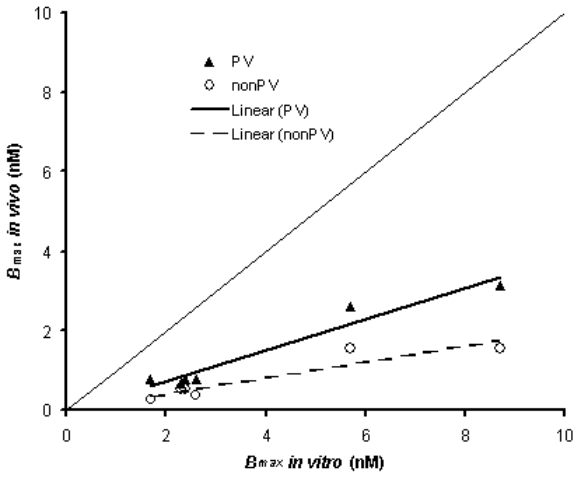

Figure 12
Correlation of *in vitro* and *in vivo* measures of receptor concentration with and without partial volume (PV) correction. The line of identity is indicated.

This agreement is in line with a study involving a direct comparison of [^{11}C]SB207145 binding measured by PET in the minipig, with subsequent [^{3}H]SB207145 postmortem autoradiography and binding assay measurements in the same pigs [42]. Although the rank-order between *in vivo* and *in vitro* B_{max} was significant, the *in vitro* B_{max} using [^{3}H]GR113808 [50] were five-fold larger (two to three-fold when applying PV correction) than in our PET study of human brain. Several causes for the disagreement are possible, which is often seen [51;52]. First, the *in vitro* measures could be noisy as the delineation of the regions e.g. the inclusion of different cortical layers *in vitro* will affect the measured B_{max}. Consequently, small errors in the challenging measure of specific activity of tritium-labeled ligands will lead to proportionally large errors of B_{max}. Second, the *in vivo* measures are biased by partial volume effects and the use of SRTM in high binding regions as shown in **study IV**. In conclusion, it is difficult to compare directly quantitative PET data with gold standard *in vitro* data as variations between *in vitro* experiments with different ligands can also vary several-fold.

APPLICATION TO MYELINATED WHITE MATTER FIBERS

The myelinated fibers of the central nervous system are crucial for fast and synchronized neurotransmission and changes in the myelination or disruption of the fiber tracts will consequently affect normal brain function. An approach for investigating the integrity of fibers is diffusion weighted imaging, an MRI method that measures the diffusion of water molecules. The restriction of diffusion within white matter tracts can give a measure, known as fractional anisotropy, of the amount of myelinated fibers. This approach has been used for studies of aging, which tend to show a decrease in the amount of myelinated fiber tracts in the white matter with age [53]. Quantitative autopsy studies of the white matter are scarce and often

restricted to smaller regions like the corpus callosum where 2D counting is possible because all fibers are parallel [54-56]. The total length of nerve fibers can be assessed from the entire white matter using stereologic methods based on unbiased principles. Only the myelinated nerve fibers were studied, which constitute the majority of nerve pathways in brain white matter in the central nervous system in contrast to the peripheral nervous system [57].

A stereologic method [58] was used to estimate the total volume, total length, and the diameters of white matter myelinated nerve fibers in autopsied brains in **study I, II,** and **III**. The method is based on the isector principle [59], which is a method for generating isotropic uniform sections planes by embedding the small tissue samples into spheres. The method has later been shown to be applicable for cortical myelinated fibers in rats as well [60]. A preliminary study of five young and five old human women [61] had showed a decrease of the total length of myelinated fibers with age. White matter biopsies were sampled uniformly randomly: One hemisphere was sectioned into slabs and approximately eight slabs were sampled uniformly at random. A plastic sheet with equidistantly spaced holes (6.8 cm^2 per hole) was then placed randomly on the caudal surface of the sampled slabs, and 1-mm needle biopsy samples were obtained where the holes in the sheet contacted the white matter (figure 13).

This biopsy technique ensures a uniformly random distribution of the white matter samples and, thereby, provides an equal sampling probability for all parts of the white matter. Thus, the final total number of samples represented all parts of the white matter equally.

The tissue was embedded in three-mm Epon spheres, and the spheres rotated randomly before re-embedding [59]. This procedure ensures isotropic, uniform, and random sections, so that each biopsy sample has a uniformly random orientation before cutting. This approach is essential to avoid bias in the length measurements due to the polytropic orientation of the myelinated fibers. Very thin sections (100 nm) were cut from each biopsy specimen to decrease the projection bias.

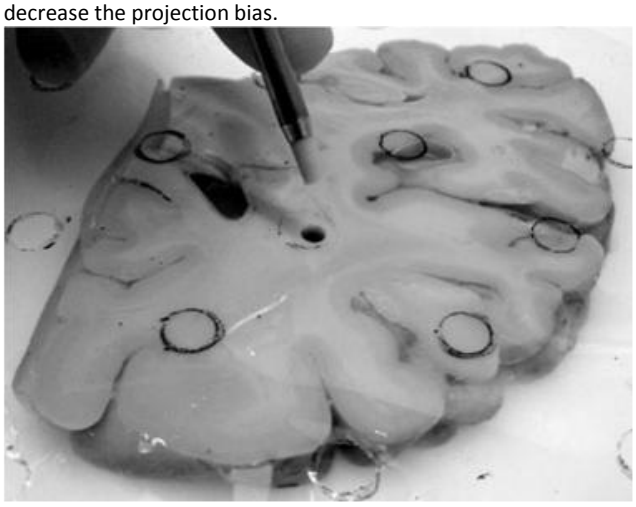

Figure 13
Sampling of biopsy specimens. A grid with equidistantly spaced holes on top of a slab of brain. The tissue is biopsied where the holes hit white matter (from **study I**).

As the thinnest myelinated fibers are only two to three times thicker than the sections, a small overestimation of the volume density must, however, be expected [29]. The unbiased counting frame was used for counting the length density at a total magnification of approximately 10,000× (figure 14) and the diameter of each fiber was measured to the nearest 0.1 µm. The myelin sheath is rather unaffected by postmortem autolysis and was therefore used as the counting item. When studying older subjects, 26% of the sections turned out to be gray matter (around 50%) or were excluded due to artifacts such as bubbles, cracks and poor staining (around 50%), a circumstance which held for Alzheimer patients as well.

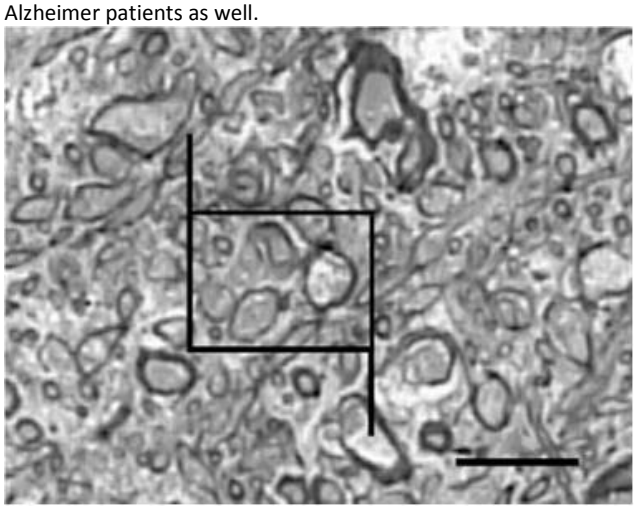

Figure 14
Fibers counted at approximately 10,000× magnification by using light microscopy and an unbiased counting frame. Scale bar 5 µm (from **study I**).

Around 3-400 fibers were counted per brain with an average coefficient of error (*CE=SEM*/Mean) of around 0.10 for the estimate of the total length. The variance between the sections determines the minimum required number of sections per brain, and the variance between the counting frames in each section determines the optimal number of counting frames. A coefficient of error of approximately 10% was regarded as optimal. Larger errors would mean that the data are too uncertain, and lower errors would indicate that the extra labor would have been spent more efficiently by studying a larger number of brains, as the biological variance is very high. To ensure that the identification of nerve fibers was reliable and reproducible, three brains were recounted. The densities of the brains were 261, 237 and 288 m/mm^3 at the first counting and 268, 277, versus 285 m/mm^3 at the second. This difference was deemed negligible.

To measure the shrinkage, three extra biopsy samples from each brain were sampled. They were sampled just adjacent to three of the earlier sampled biopsy specimens chosen systematically at random. A small cube of tissue was cut out, and a needle biopsy was performed from the cube in sagittal, frontal, or horizontal orientation so that each brain was represented by all three orientations. The top one-mm cylinder of white matter was carefully separated from the rest of the cylinder and the cross-sectional area was measured in a light microscope. The cylinders were fixed and dehydrated together with the rest of the specimens from that particular brain. Sectioning was performed perpendicularly to the length of the cylinder. After staining, the area was measured again and the area shrink-

age was then calculated. The average area shrinkage was found to be 5.9% ($p< 0.001$) in **study I**, 9% in elderly control cases and AD patients in **study III**, and 9% in schizophrenic patients in **study II**, which were significantly different from the 16% in the age-matched control cases (p=0.009) in **study II**. No dependency of orientation was found in any of the studies. In **study I** and **III**, the average shrinkage was used to correct the length density estimates, while in **study II**, separated corrections were used for schizophrenic patients and control cases. The difference in processing-related shrinkage between the schizophrenic and the control brains might likely be due to a longer storage time of the schizophrenic brains, such that vigorous measuring and correcting was necessary to avoid bias in such material. Indeed, the differential shrinkage artifacts are a major limitation for the studies. The studies were performed in different time periods and by different technicians; identical methods should have yielded identical shrinkage. The correcting term was included in the calculation of the length density:

$$L_V = \frac{2 \times \text{Total number of counted nerve fiber profiles}}{\text{Total sampling area} \times (1 + \text{average area shrinkage})}$$

The total length is estimated by multiplying with the white matter volume (V_{WM}):

$$\text{Total length} = L_V \times V_{WM}$$

Myelinated Fibers in Aging

The interest in white matter changes in the healthy aging process has increased dramatically following the initial demonstrations by magnetic resonance imaging (MRI) of significant age-related cerebral white matter changes. The percent of a healthy aged population showing one or more hyperintense lesions on T2-weighted images increases almost linearly from below 20% for individuals 21–30 years of age to 100% for individuals 71–80 years of age (n=142)[62]. These changes are especially prevalent in individuals with Alzheimer's disease or vascular dementia, and are likely to be caused by ischemia. In general, the hyperintensity lesion is a rather nonspecific change, as almost any change in tissue composition will increase the water content and, thereby, produce a hyperintense signal [63]. It is microscopically characterized by a rarefied appearance of the white matter; loss of myelin, axons, and oligodendrocytes; as well as stenosis of arterioles and smaller vessels similar to that found at the border of true infarcts [64].

A neuropathological quantitative study of human aging using stereological methods has shown minor age-related declines in total neocortical neuron number by 10% and neocortex volume of 13% as compared to a much larger decline in white matter volume by 28% [4]. *In vivo* studies using MRI also reveal significant age-related losses of white matter volume compared with a much smaller decline in gray matter volume [65;66] at least in old age [67]. A combined study of diffusion tensor imaging and white matter volume in 430 subjects aged 8 to 85 years revealed a peak in fractional anisotropy around 30 years of age and a peak of white matter volume around 50 years of age [53]. Loss of fractional anisotropy could be caused by loss of fibers, change in size, or disruption of the myelin sheath. The combination of loss of white matter with an increasing number of white matter lesions suggests a loss of nerve fiber in the aging process.

To evaluate age and sex effects, a material of 36 brains (18-93 years of age, 18 men) was studies using the method described above (**study I**). All subjects were had normal activities of daily living until shortly before death despite some chronic medical conditions. Although no cognitive assessment had been performed, the hospital staff or their local practitioner regarded them cognitively normal and a thorough neuropathological examination was performed to exclude neurological disease. Using the stereological method described above, men were found to have a total length of 176,000 km of myelinated fibers at age 20 and 97,200 km at the age of 80 years. Women were found to have a total fiber length of 149,000 km at age 20 and 82,000 km at age of 80 (table 2).

A regression of the total length of nerve fibers as a function of age revealed negative regression coefficients significantly different from zero in both men (p=0.0007) and women (p=0.00008). Men were found to have 16% longer total length of myelinated fibers (p=0.02) compared to women, which likely corresponds to a 16% difference in total neocortical neuron number [4]. The sexes showed no difference (p=0.32) in the relative loss, which was 10% per decade or 45% from the age of 20 to 80 years (figure 15).

Four subjects had significant neuropathological changes, characterized by scattered senile plaques and amyloid deposits, although no signs of dementia were reported. Removing these subjects from the analyses did not change the results significantly.

Table 2

Results of white matter myelinated fibers

	Sex	20 years	80 years	Age diff. pr. Decade	Sex diff.
Total length (km)	**Men**	**176,000**	**97,200**	**10%*** **	**16%***
	Women	**149,000**	**82,000**	**10%****	
Fiber length density (km/mL)	**Men**	**321**	**229**	**5,8%****	**3,5%**
	Women	**310**	**221**	**5,8%*** **	
White matter volume (mL)	**Men**	**550**	**423**	**4,3%**	**13%***
	Women	**484**	**372**	**4,3%***	

* p<0.05, **p<0.01, ***p<0.001, ****p<0.0001.

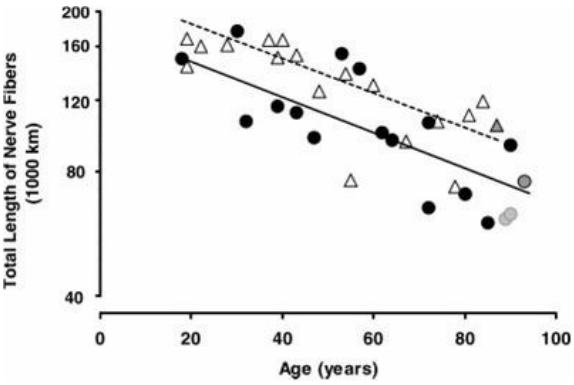

Figure 15
Total length of myelinated fibers on a logarithmic scale as a function of age for men (triangles) and women (circles). The regression lines with a common slope of 1% per year are indicated for men (dashed line) and women (solid line). The subjects showing neuropathological changes in the hippocampal region are depicted by the gray filled triangle and encircled gray circles, whereas the subjects with changes in the cortex as well are depicted by non-encircled gray circles.

The analyses of fiber diameters showed an increase with age in geometric mean diameter of 13% (p= 0.005) with age from 0.79 μm at the age of 20 years to 0.89 μm at the age of 80 years for both sexes. The size distribution for young and old subjects of each sex is shown in figure 16, which suggests a loss of the fibers smaller than 1.5 μm but no gain of the thicker ones; hence, small diameter fibers are dropping out not getting thicker. The age-adjusted distribution showed no difference in geometric mean fiber diameter between men (0.86 μm) and women (0.85 μm; p=0.95). Thus, the reduction of total smaller fiber length increases progressively from the age of 20 years.

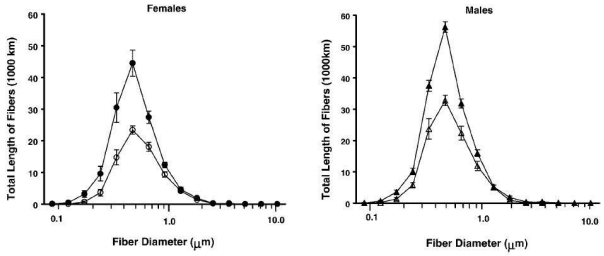

Figure 16
The total length of myelinated fibers is shown as a function of diameters on a logarithmic scale. Left are "young" (≤ 45 years, filled circles, n=5) and "old" (≥70 years of age, open circles, n=8) women. Right are "young" (≤ 45 years, filled triangles, n=8) and "old" (≥70 years of age, open triangles, n=5) men. Error bars represent one standard error (from study I).

It should be emphasized that these findings relate to the myelinated fibers. We have no data regarding the unmyelinated fibers, and the loss of white fiber length could theoretically be a result of demyelination with preservation of bare axons. The loss of total fiber length with age is due to a 23% decrease in white matter volume and a 29% decrease in length density, i.e., fiber length per volume. Hence, measuring the total length of myelinated fibers reveals a much more pronounced age-related loss than the previously described loss of white matter volume would indicates. Part of this loss could be due to secular trends. During the past century, the brain has increased in size in proportion with the rest of the body. Recordings of body and brain weights of 7397 autopsied individuals aged 20-50 years from London report an increase in brain weights of approximately 5% in subjects born around 1860 compared to subjects born around 1940 [68]. Most likely, secular trends can explain up to 5% of the changes in total length of nerve fibers with age, whereas the remaining 40% probably is an actual decrease in the number of neuronal connections.

The analyses of fiber diameters showed an increase with age in geometric mean diameter of 13% (p= 0.005) with age from 0.79 μm at the age of 20 years to 0.89 μm at the age of 80 years for both sexes. The size distribution for young and old subjects of each sex is shown in figure 16, which suggests a loss of the fibers smaller than 1.5 μm but no gain of the thicker ones; hence, small diameter fibers are dropping out not getting thicker. The age-adjusted distribution showed no difference in geometric mean fiber diameter between men (0.86 μm) and women (0.85 μm; p=0.95). Thus, the reduction of total smaller fiber length increases progressively from the age of 20 years.

It should be emphasized that these findings relate to the myelinated fibers. We have no data regarding the unmyelinated fibers, and the loss of white fiber length could theoretically be a result of demyelination with preservation of bare axons. The loss of total fiber length with age is due to a 23% decrease in white matter volume and a 29% decrease in length density, i.e., fiber length per volume. Hence, measuring the total length of myelinated fibers reveals a much more pronounced age-related loss than the previously described loss of white matter volume would indicates. Part of this loss could be due to secular trends. During the past century, the brain has increased in size in proportion with the rest of the body. Recordings of body and brain weights of 7397 autopsied individuals aged 20-50 years from London report an increase in brain weights of approximately 5% in subjects born around 1860 compared to subjects born around 1940 [68]. Most likely, secular trends can explain up to 5% of the changes in total length of nerve fibers with age, whereas the remaining 40% probably is an actual decrease in the number of neuronal connections.

The large reduction in connections is matched by only a moderate (10%) loss of neocortical neurons by 10% [4], such that a primarily loss of the long projections or collaterals could theoretically explain part of the high loss of fiber length with age. However, a larger (30%) age-related loss of synapses is found in aged monkeys [69], supporting a general age-related loss of connections between otherwise preserved neurons. The white matter could be the pathological site for this loss, as numerous studies of myelin sheaths in monkeys (for a review, see [70]) show that oligodendrocytes rather than neurons are affected by age [71] and that the myelin sheath can degenerate while leaving the axon is intact. Furthermore, evidence suggests that the oligodendrocytes are very susceptible to ischemia and potentially cytotoxic substances produced by the microglia such as cytokines and nitric oxide [72]. Conceiva-

bly, cerebral small vessel changes could result in an inability of the oligodendrocytes to maintain the sheaths.

Possibly, the substantial loss of white fibers in the aging brain could plausibly be of importance in the declining cognitive functions seen in elderly people due to the lower propagation velocity for impulses accounts for slower activity in some brain functions [70].

Myelinated Fibers in Schizophrenia

Though the data from neuropathology are variable, evidence speaks for a dysfunction of the prefrontal cortex being part of the etiology of schizophrenia. The particular interest in frontal lobe abnormalities in schizophrenia is derived from observations in these patients of cognitive and behavioral deficits that are associated with frontal lobe damage, e.g. Wisconsin Card Sorting Task, eye-tracking abnormalities [73], and from functional imaging studies [74].

More specifically, the prefrontal cortex is of interest in schizophrenia. The functional definition of the prefrontal cortex includes its reciprocal interactions with the mediodorsal nucleus of thalamus, which is indeed one of the primary subcortical structures linked to the prefrontal cortex from schizophrenia patients [75]. Stereological cell counting show consistently no change of total neuron number in the entire prefrontal cortex from schizophrenic patients [76;77] but revealed highly varying findings for total neuron number in the mediodorsal nucleus of thalamus, where losses were 30–40% in one study [78], or no difference in another study of similar design [79], for a reviews see [75].

A few studies have measured the prefrontal white matter selectively with conflicting results: some report a significant reduction by 3, 8, or 15% [80-82], while others report non-significant reductions by 1–3% [83-86]. There is, however, no consensus on the demarcation of the prefrontal white matter, and the volume estimates varies remarkably from 42 to 145 ml. The study with the largest number of patients (159 schizophrenic patients and 158 control cases) reports a significant reduction by 3% [82]. It is, however, questionable whether a reduction of less than 5% can be of biological significance.

To study the white matter connections, MRI diffusion tensor imaging has increasingly been used, and although the findings have been somewhat inconsistent, frontal and temporal abnormalities are often reported [87]. Post-mortem microscopy of myelinated fibers in the corpus callosum using stereological methods showed a significant decrease in the number of fibers in female schizophrenic patients but not in male patients [54], and no differences was found in the total number of fibers in the fornix of schizophrenic patients as compared to control cases [88].

The total length of myelinated nerve fibers was estimated in both the global white matter and the prefrontal white matter in eight brains from chronic male schizophrenic patients (mean age 60.3±14 years) and nine control cases (mean age 59.7±14 years) in **study II**. The schizophrenic patients fulfilled the criteria for the DSM III classification and belonged to a subpopulation of severely ill patients, hospitalized for a substantial part of their lives and treated with neuroleptic treatment, insulin comas, or electroconvulsive therapy (ECT). Three developed tardive dyskineasia and five became demented. A simple and reproducible method for delineating the prefrontal white matter was applied: the prefrontal white matter was defined as terminating in the second slab containing the temporal lobe, when slabs were cut from the frontal pole.

We found no difference in schizophrenic patients in total length of myelinated fibers globally and prefrontally (table 3). Furthermore, the size distribution of the fibers in schizophrenics was within normal limits as compared to control cases (figure 17).

Table 3

White matter myelinated fibers in patients with schizophrenia and control cases

		Schizo	Controls	Diff.	95% c.i.
Total length (1000 km)	Global	129 ±21.9	137 ±35.6	-6.1%	-30% to 17%
	Prefrontal	25.7 ±10.0	27.6 ±9.38	-7.2%	-44% to 30%
Density (1000 km/mL)	Global	0.296±0.015	0.270±0.030	9.4%*	0.58% to 18%
	Prefrontal	0.295±0.053	0.296±0.050	-0.1%	-18% to 18%
White matter volume (mL)	Global	434±60.8	507±122	-16%	-37% to 6%
	Prefrontal	85.9±29.2	93.0±25.1	-8,0%	-39% to 23%
Geometric mean (μm)	Global	0.86 ±0.077	0.86 ±0.052	-0.1%	-6.8% to 6.6%
	Prefrontal	0.82±0.033	0.82±0.049	0.4%	-4.2% to 4.9%

* p<0.05.

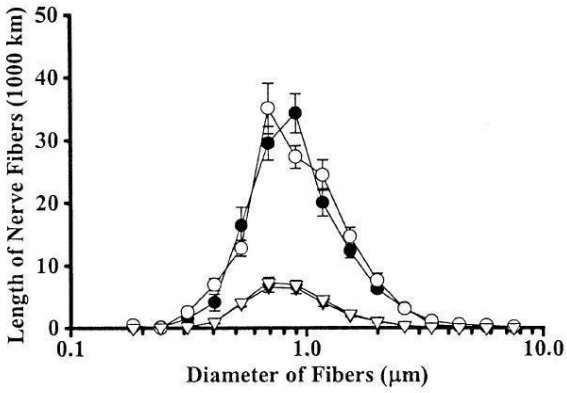

Figure 17
Distribution of fiber length versus diameter. The mean length of fibers for each group of fiber diameters were calculated for schizophrenic patients in global white matter (filled circles), for schizophrenic prefrontal white matter (filled triangles), for control cases globally (open circles), and for control cases prefrontally (open triangles). The scale is semilogarithmic, so as to approach a normal distribution. The standard errors of the means are indicated (from study II).

Our findings do not support an elevated loss of myelinated nerve fibers in the brain white matter or prefrontal white matter of patients with chronic schizophrenia. Similarly their size distributions were not statistically significantly different from those of control cases. A limitation of **study II** is due to the limited number of brains, as required by the time consuming stereological method and the need to deal with a homogenous material: All the schizophrenic patients were severely affected and had spent a substantial number of years in psychiatric wards, and only men were included, as the sex difference was 17% (**study I**). As noted above Highley and coworkers found a significant reduction in corpus callosum fibers in female schizophrenics but not in male schizophrenics [54]. Therefore, to make overall conclusions on schizophrenics, the study has to be repeated for women, as they may show other structural changes than men. A limitation of the total prefrontal fiber length quantitation is the rather arbitrary definition of the prefrontal white matter. According to Groenewegen, three different criteria have been used for the anatomical demarcation of the prefrontal cortex [89]: the cytoarchitectonic, the mediodorsal thalamus projections, and dopaminergic innervation. However, the prefrontal cortex is relatively consistently defined as Brodmann areas 8–12, 24, 32, 46 and 47 [90], which more or less comprise the frontal lobe without the primary motor and premotor areas. In contrast, the prefrontal white matter cannot be unambiguously delineated. We chose arbitrarily to define the posterior demarcation of the prefrontal white matter at the beginning of the temporal lobe, i.e. the first slice including the temporal lobe is the last slice of the prefrontal white matter. This definition of the prefrontal white matter excludes the posterior half of the anterior cingulate cortex (areas 24 and 32) that extends further back than does the rest of the prefrontal cortex, and it may include the most anterior parts of the motor association areas. Others have chosen the slice just anterior to the lateral ventricles [83] or the first slice that included the corpus callosum, but given that ventricles and corpus callosum may be altered in schizophrenia [54], these definitions are not optimal either. Shrinkage of temporal lobe structures in schizophrenics could bias our delineation of prefrontal white matter, but the prefrontal white matter made up 20% of the global white matter in schizophrenic as well as control brains.

Our findings show that stereological methods with measurements of both length density and volume are necessary, as the density was increased and the volume reduced in schizophrenics, which tend to cancel out when calculating the total length.

Myelinated Fibers in Alzheimer's Disease

As many as 7% of people older than 60 years have Alzheimer's disease (AD), which has motivated increased attempts to understand the pathogenesis of the disabling cognitive dysfunction of the disease. The hallmark of neuropathological findings of AD are an isocortical extracellular accumulation of β-amyloid polypeptide in plaques and a subsequent appearance of intraneuronal neurofibrillary tangles containing tau protein, which first appear in the mesial temporal lobe and spreads to the rest of the cortex as the disease advances [91].

Apart from the cortical changes, white matter changes may be involved in AD. Neuropathological findings in AD include deep white matter lesions [64] and MRI shows an increasing prevalence of hyperintense lesions on T2-weighted images, the extent which correlates to cardiovascular risk factors [92]. The hyperintense lesions may be slightly more prevalent in AD than in healthy aging [93], possibly due to microvascular dysfunction because of circulating β-amyloid polypeptide [94].

Volumetric studies of white matter volume in AD patients have not yielded consistent findings. Post mortem studies show no global white matter reduction in AD [95;96], which could be due to an accelerated white matter reduction in old age [67;97] thus limiting the difference between AD patients and age-matched control cases when studying aged AD patients. Thus, a post mortem study found a significant decrease of white matter in patients with AD only when patients and control cases were below the age of 80 [98]. White matter atrophy has been reported to be selectively confined to the temporal lobe of AD patients in an MRI study using voxel based morphormetry [99] and to the temporal, inferior parietal and rostral frontal white matter using a regional parcellation method [93]. Furthermore, the latter study also reported changes in fractional anisotropy in the temporal lobe, suggesting loss of connectivity and fiber tracts.

The global total number of neocortical neurons has been estimated using stereological methods in eleven AD subjects and compared to ten control subjects without neurological disorders [96]. The total neocortical neuron number was 16.9×10^9 in the AD patients, which was not statistically significantly different from the 18.1×10^9 count in the control group. This study has since been repeated including also the estimation of the total neocortical glia cell numbers [95]. The second study confirmed that num-

bers of neurons and glia cells are the same in subjects with AD compared to age-matched control subjects.

The aim of **study III** was to estimate the total myelinated white matter fiber length and the average diameter of the myelinated nerve fibers in brains of subjects with AD as compared to control subjects. The material consisted of brains from eight women with AD (mean age 83, range: 79-88 years) and ten women as control cases (mean age 84 years, range: 74-92 years). All the demented patients came from Department of Psychogeriatry in Copenhagen, Denmark, and all had been evaluated prospectively with a psychometric dementia test and neurological examinations once a year during their last years of life and the material comprised only brains from the most severely demented Alzheimer women.

The pathoanatomical diagnosis of AD was based on the presence of numerous widespread senile plaques in the neocortex shown after application of a silver stain, but the isocortex also showed tangles and amyloid angiopathy comparable to Braak stages V and VI [91]. Five of the ten control cases had few scattered plaques in neocortex and one had both plaques and vascular amyloid deposits in neocortex but no tangles; this pattern is also be seen in normal aging [100]. This control subject was an 89 year old woman with no sign of dementia, dying suddenly of a myocardial infarction but it cannot be excluded that she in fact had early AD.

The mean total length of nerve fibers in white matter was 81,600 $\pm$ 14.5 km in the AD group showing no significant difference compared to the control cases 78,900 $\pm$ 18.7 km (p=0.75) (figure 18). The mean fiber length density was 248 $\pm$ 33.6 km/cm^3 in the AD group and almost the same 247 $\pm$ 45.0 km/cm^3 in the control cases (p=0.98). The white matter volume in AD patients was 329 $\pm$ 35.6 cm^3 and 321 $\pm$ 58.8 cm^3 in control cases (p=0.74). The average geometric diameter was 1.03 µm (AD) and 1.02 µm (control) (p=0.23) and figure 19 shows the rather similar diameter distributions for the AD and control cases.

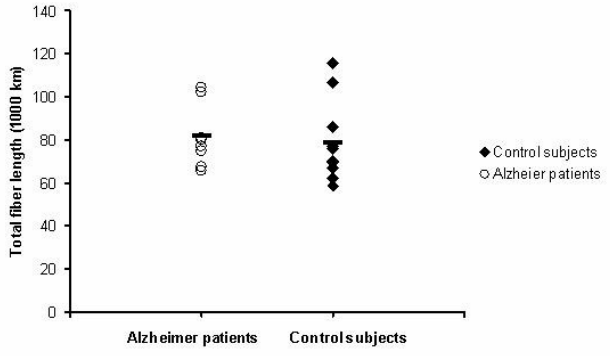

Figure 18
The total fiber length for AD patients and control subjects (from study III).

The limitation of study III is again the small sample size. The massive loss of fibers in normal aging of 45% could limit the power to detect a possible further loss in AD. However, smaller differences are however unlikely to be of major importance in the pathology of AD. We had a rather high rate of biopsies that were excluded due to technical low quality or because they did not contain white matter. However, the sampling of biopsies not containing white fibers or with artifacts was not different in any systematic way compared to the biopsies from the control cases. Furthermore, because of a sufficiently high primary sampling fraction, the remaining number of biopsies was more than sufficient to meet our requirement for precision.

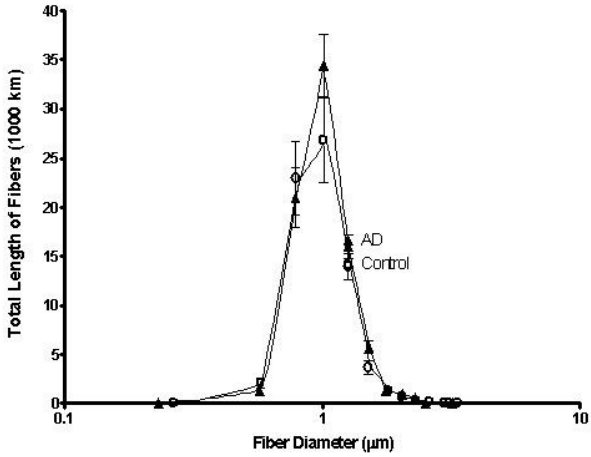

Figure 19
The diameter distribution of fibers for AD patients (filled triangles) and control cases (open circles). The total length of myelinated fibers is shown as a function of diameter on a logarithmic scale. The standard errors are indicated (from study III).

The recent report of increased amounts of white matter lesions as reported by [93] is not necessarily in contrast to our findings. The lesions observed using MRI are most likely of vascular origin, and thus due to localized damage. The aim of **study III** was to evaluate possible changes in all white matter to study if part of the symptoms in AD could be due to widespread white matter changes not detectable by MRI. We sampled around 10 biopsies of white matter, which is not sufficient for evaluation of localized white matter lesions. Thus, our findings do not support generalized white matter changes but do not rule out localized areas of white matter damage.

The lack of difference in white matter parameters between AD patients and control subject was surprising. It is in line, however, with the previous findings in the same brains [95;96] of normal neocortical cell numbers, since we would expect a neocortical neuron loss to be followed by a reduction in the total length of myelinated fibers. Our results surprisingly suggest that very basic structural elements such as the total global number of neocortical neurons and glia cells and the total length of the myelinated fibers are more or less unaffected in AD.

APPLICATION TO SEROTONIN RECEPTORS AND TRANSPORTERS

Pharmacologically, the focus on the serotonin system has increased by the widespread use of the antidepressant medicications of the class 'selective serotonin reuptake inhibitor' (SSRI), which block the serotonin transporter (5-HTT) located presynaptically on projecting serotonergic axons, thereby increasing the interstitial serotonin concentration. In addition, the 5-HT$_{2A}$ receptors are targets for medications used to treat conditions such as schizophrenia, anxiety, depression, and Parkinson's disease. Moreover, most hallucinogens mediate their effects through the 5-HT$_{2A}$ receptor [101].

A well-documented decrease of 5-HT_{2A} receptor binding is seen in PET studides of AD [102;103], whereas normal aging is associated with a decrease of 6-8% per decade [104;105]. Quantification of 5-HT_{2A}-receptors with [^{18}F]altanserin, a highly selective 5-HT_{2A}-receptor antagonist, can be performed with a bolus/infusion protocol where steady-state tracer levels are obtained in blood and brain [43]. A radiolabeled metabolite, altanserinol, of [^{18}F]altanserin crosses the blood brain barrier and biases the quantification using ordinary bolus techniques. This is overcome by the steady-state protocol, which enables subtraction of the non-specific binding directly and the possibility to normalize to tracer concentration in venous plasma samples. The reproducibility of the method has previously been tested in six normal men (age-range: 33-67 years) with a two week between-scan interval; the median difference between the measurements ranged from 6% in high binding regions to 17% in low binding regions [106].

The quantification of 5-HT_{2A} receptors with [^{18}F]altanserin with a bolus/infusion protocol to obtain steady-state tracer levels has been described in detail [43]. In brief, two hours after initiation of bolus plus constant infusion of tracer (bolus/infusion ratio of 1.75h), steady-state conditions are reached and series of five emission frames of eight minutes each scans are acquired with the GE-Advance scanner. Venous blood samples are drawn at mid frame times during the emission recording. The plasma activity and the fraction of unmetabolized tracer are measured using high performance liquid chromatography (HPLC) [43].

Quantification of the serotonin transporter is made using the highly selective radioligand, [^{11}C]DASB injected as a conventional single bolus, followed by a 90 min dynamic emission recording.

For applying regions of interest for quantification of both 5-HT_{2A} receptors and serotonin transporters, an MRI is acquired for each subject and segmented into gray matter, white matter, and cerebrospinal fluid. These segments are subsequently used for partial volume (PV) correction and for masking the voxels in the regions of interest. PV correction uses the anatomical information from the MRI to correct for the spill-in and spill-out between gray matter and neighboring tissue in the smoothed PET image. Both a one tissue-type method using brain and non-brain segmentation [107] and a two tissue method using gray matter, white matter, and non brain segmentation [108] are used. PV correction is particularly required in studies of aging and AD patients that are expected to differ from healthy control cases with respect to atrophy. A total of 18 bilateral regions of interest are automatically delineated on each subject's MRI in a user-independent fashion [44]. The dorsal raphe nucleus is not visible on the MRI, so its region was defined functionally on the basis of a threshold-based delineation of the radioactivity in the [^{11}C]DASB images obtained in ten healhy control subjects and included to the MRI region set [109]. In contrast to the cerebral and cerebellar regions, no masking for gray matter voxels and no partial volume correction is used in dorsal raphe nucleus so as to avoid relying on a possibly erroneous segmentation of the midbrain.

For [^{11}C]DASB, kinetic modeling is performed using the multilinear reference tissue model MRTM2 [37] with cerebellum as reference region to achieve BP_{ND}. For [^{18}F]altanserin, the outcome parameter is BP_P, using the measured metabolite corrected venous plasma. Cerebellum was used as reference region, since it represents non-specific binding only [43].

Serotonin Receptors in Aging and the Effect of Partial Volume

The stability of the steady-state method on a longer time-scale and in older individuals was ascertained to validate the use of [^{18}F]altanserin for long-term follow-up examinations in **study VI**. We obtained [^{18}F]altanserin PET recordings in twelve healthy elderly subjects at baseline and at a two-year follow-up in order to evaluate stability of measures and variability with increasing complexity of PV corrections.

In the healthy elderly individuals, there was found no change in regional 5-HT_{2A} receptor levels at two-year follow-up regardless of application of PV correction (table 4). The variability was 12-15% and the *ICC* scores were 0.45-0.67 for larger high binding cortical regions, when applying two-tissue PV corrections and 14-22% with *ICC* scores of 0.46-0.72, when no PV correction was applied. Correcting for an expected two-year decline in 5-HT_{2A} receptors of 1.7% [104;105] did not seem to diminish variability in the estimates.

Binding estimates for the orbito-frontal and anterior cingulate cortici showed higher variability and lower reliability and can not be recommended as primary volumes of interest in studies requiring high test-retest performance. The higher variability and lower reliability in anterior cingulate cortex is probably due to the small size of the structure while the the orbitofrontal cortex variability is likely due to the proximity to the air-containing orbita, which make this region more prone to coregistration errors.

The *ICC* scores compare well to those found in an earlier [^{18}F]altanserin bolus-injection test-retest study [110] and to those reported for other tracers with bolus injection [47] or bolus-infusion protocols [111]. The decrease in variability and decrease in reliability (*ICC* decreases) with increasing complexity of PV correction are notable (figure 20), and in accordance with earlier findings [106]. The lower variability does not favor applying PV correction, as the reliability was diminished as well. The variability of binding potentials for nonPV corrected and PV data are not comparable, as the between-subject variability decrease with increasing PV correction, i.e. notice the decreasing coefficients of variation (*CV*) with increasing complexity of PV correction in table 4.

Table 4:
Binding potential of [^{18}F]altanserin by region at increasing complexity of partial volume (PV) correction.

Cortical Regions	No PV correction			1-tissue PV correction			2-tissue PV correction			Gray matter volume		
	Mean Baseline BP_p (*CV*)	Mean 2-year follow-up BP_p (*CV*)	Relative diff. ±*SD*	Mean Baseline BP_p (*CV*)	Mean 2-year follow-up BP_p (*CV*)	Relative diff. ±*SD*	Mean Baseline BP_p (*CV*)	Mean 2-year follow-up BP_p (*CV*)	Relative diff. ±*SD*	Mean Baseline cm^3 (*CV*)	Mean 2-year follow-up cm^3 (*CV*)	Relative diff. ±*SD*
Orbito-frontal ct.	0.83 (38%)	0.79 (42%)	2.2% ±0.38	1.35 (30%)	1.31 (34%)	1.2% ±0.30	1.85 (27%)	1.84 (27%)	3.8% (0.25)	18.1 (8.4%)	17.7 (10%)	-2.4% (0.06)
Parietal Cortex	0.88 (27%)	0.80 (28%)	-6.9% ±0.23	1.86 (23%)	1.76 (20%)	-2.8% ±0.21	3.10 (22%)	2.98 (20%)	-1.6 (0.20)	52.0 (5.7%)	51.0 (4.5%)	-1.8% (0.03)
Temporal Cortex	1.02 (27%)	0.97 (26%)	-2.9% ±0.18	1.59 (24%)	1.56 (21%)	0.0% ±0.17	2.25 (22%)	2.23 (17%)	1.3% (0.16)	72.7 (6.9%)	70.6 (7.3%)	-3.0%*** (0.02)
Ant.-cing. Cortex	0.93 (36%)	0.81 (36%)	-9.6% ±0.25	1.23 (34%)	1.11 (32%)	-4.6% ±0.28	1.85 (27%)	1.70 (25%)	-3.8% (0.27)	5.02 (6.4%)	4.86 (4.7%)	-3.1%* (0.05)
Occipital Cortex	1.04 (28%)	1.04 (24%)	2.2% ±0.19	1.56 (28%)	1.57 (22%)	4.0% ±0.19	2.90 (28%)	2.95 (19%)	5.2% (0.19)	46.7 (5.9%)	45.6 (7.2%)	-2.5%* (0.03)
Frontal Cortex	0.81 (30%)	0.76 (28%)	-4.0% ±0.21	1.75 (22%)	1.71 (19%)	0.1% ±0.20	2.72 (21%)	2.67 (15%)	1.1% (0.19)	87.9 (7.6%)	86.1 (6.6%)	-2.0%* (0.03)

The mean binding potentials (BP_p) and coeffcient of variations (*CV*= *SD*/mean) for baseline and two-year follow-up for six cortical regions with no, one-tissue [107] and two-tissue [108] PV correction and the relative differences = (scan2-scan1)/scan1 and standard deviations are reported. Significant volume reductions over two years: *p<0.05, **p<0.01, ***p<0.001.

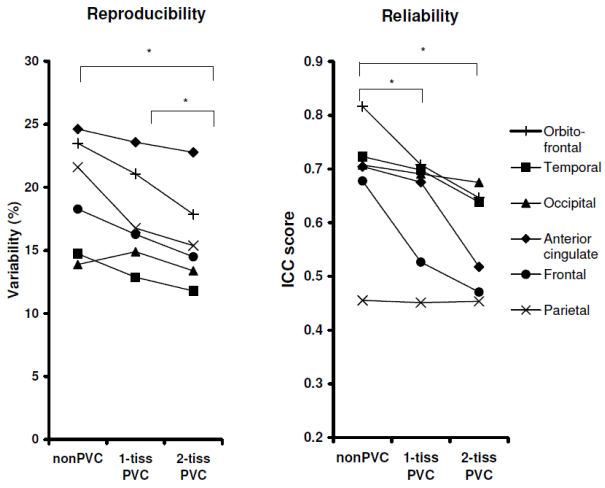

Figure 20
The effect of no, one-tissue and two-tissue partial volume correction on two-year test-retest variability (variability=|scan2-scan1|/mean(scan1,scan2) (the lower the better) (left) and intraclass correlation coefficients (*ICC*) (the higher the better) (right) of the binding potential of [^{18}F]altanserin. Both two-year test-retest variability (p=0.016) and *ICC* (p=0.047) are significantly declining with increasing PV correction (Wilcoxon signed-rank test), thereby contradicting each other. * p<0.05.

When applying PV correction, the radioactivity attributed to a thin cortical region (C_T) such as parietal cortex increases by a factor of 3.7, while the concentration in cerebellum (C_{ND}) that has little white matter and is relatively large only increased by a factor of 1.2. Thus, relative differences decrease since the subtraction term, C_{ND}, remains essentially constant (BP_P=(C_T-C_{ND})/C_P), and both within-subject and between-subject variability decrease as a function of increasing complexity of PV correction. The lower reliability when applying PV correction is most likely partly due to the lower between-subject variability (when $MSS_{Between}$ goes down, *ICC* goes down as well), and also in part due to the greater noise arising from greater influence of the imperfect coregistration of the PET and MRI. However, low between-subject variability and thereby diminished reliability does not inherently decrease the chance of detecting differences between groups, although the expected differences between groups should be dependent on whether PV correction will be applied. In studies requiring high test-retest performance, PV correction is not to be recommended, but should on the other hand not be disregarded in studies of degenerative diseases with anticipated atrophy. PV correction remains the only method that allows for a distinction between BP_P changes due to atrophy and due to changes in binding of receptors, given the low resolution of existing PET relative to the cortical thickness.

The reduction of gray matter volume over two years (table 4) may partly be explained by an age-related atrophy of gray matter and partly by a lowering of the water content in the gray matter with age [112], which biases the segmentation of gray and white matter. We used templates for the segmentation which were derived from relatively young subjects (Montreal Neurological Institute, MNI) in whom there was higher contrast compared to that in the elderly; this could call into question the reliability of our segmentation. However, the robustness in test-retest was found to be high with *ICC* scores of 0.74-0.87 and the segmentation did not seem to bias our findings, as no change in binding potentials over two years were observed regardless of application of PV correction. Thus, the observed variability between the MRIs at baseline and two-year follow-up will only account for some of the variability observed. A more pronounced contribution to variability is likely arising from image processing, as the manual coregistration method show higher variability as compared to the automated methods, but perhaps less bias. As the steady-state method for [^{18}F]altanserin does not provide early cerebral blood flow-like tracer uptake images well-suited for automated coregistration, a manual method was chosen for [^{18}F]altanserin to avoid bias. This increases the variability as compared to what is typical for dynamic protocols. Variability in the fitting and modeling of tracer uptake in dynamic scans is likewise dependent on the number of manual steps in the analysis. It must be stressed that low variability in the processing by using automated methods does not increase the accuracy of data and automated methods should always be carefully evaluated for possible biases and a trade-off between bias and variability chosen.

Our findings support a stable 5-HT$_{2A}$-receptor level over two years in healthy aged individuals, which is in accordance with the finding in monozygotic twins of high showing a high degree of covariability of 5-HT$_{2A}$ receptor density compared to dizygotic twins [113].

Serotonin Transporters in Alzheimer's Disease

Symptoms of depression, aggression, anxiety and disturbances in food intake and sleep are common in AD and serotonergic impairment is well documented in that condition. Post mortem brain studies of patients who had AD have consistently found significant loss of serotonergic neurons or reductions in the plasma membrane serotonin transporter (5-HTT) in the raphe nuclei [114-117]. Also the serotonergic neuronal projections to subcortical and neocortical structures are reduced in densitiy in post mortem specimens from the mesial temporal lobe [116] as well as neocortical regions [118;119]. Reductions in both 5-HTT [120]. Further, postsynaptic receptor subtypes have been documented in several postmortem studies (5-HT$_{1A}$ [121], 5-HT$_{2A}$ [122-125], and 5-HT$_6$ [125]). *In vivo* imaging studies with PET also show reductions in cerebral 5-HTT [126], 5-HT$_{1A}$ receptor [127-129], and 5-HT$_{2A}$ receptor [103;130], binding, the 5-HT$_{2A}$ receptor binding was reduced even in very early AD patients [102].

In a study of patients with amnestic mild cognitive impairment (aMCI), the precursor for AD, we found a 20-30% global reduction in 5-HT$_{2A}$ binding which is comparable to a 30% reduction found in the study by Meltzer et al. [103]. This finding suggests that reductions in 5-HT$_{2A}$ are widespread and occur even before the onset of frank AD [102]. The reason for this reduction remains obscure, but may be an indicator of atrophy of cortical pyramidal neurons on which the receptors are expressed.

The aim of **study VII** was to determine whether the reduction in 5-HT$_{2A}$ receptor binding in AD can be attributed to a specific dysfunction of the projecting serotonergic neurons and their projections, or of it is an unspecific marker of cortical neuronal dysfunction. To this end, we

combined [^{11}C]DASB and [^{18}F]altanserin recordings in a series of 12 patients with AD and 11 healthy sex- and age-matched subjects, and carried out analyses of regional binding to 5-HTT and 5-HT$_{2A}$ receptors.

The mean binding potentials for [^{18}F]altanserin and [^{11}C]DASB from these subject groups are shown in table 5 and the binding maps for the two tracers is illustrated for a representative patient and one healthy subject in figure 21.

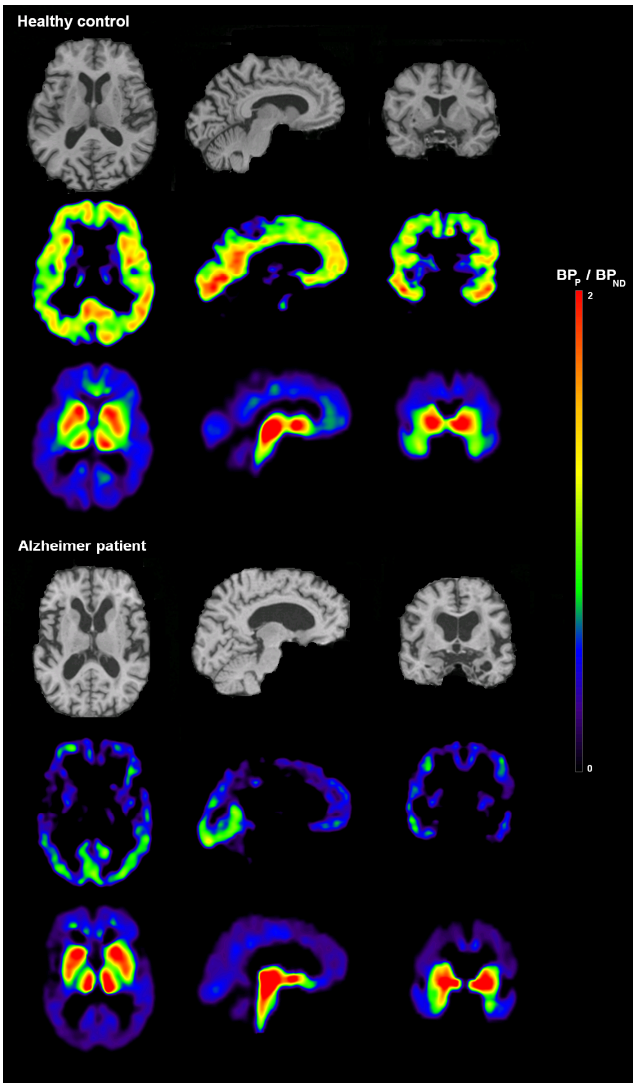

Figure 21
Parametric maps [^{18}F]altanserin and [^{11}C]DASB] in a representative healthy control case (upper rows, 73 years, male) and AD patient (lower rows, 73 years, male). The three rows for each subject consist of an MRI, a 5-HT$_{2A}$ receptor parametric image, and a serotonin transporter parametric image. From left to right, the sections are: horizontal (through the caudate nucleus and putamen), sagittal (through the midbrain), and coronal (through the caudate nucleus with mesial temporal cortex just below).

A marked global reduction in neocortical 5-HT$_{2A}$ receptor binding in the AD group (p=0.02) was not associated with a similar decrease in 5-HTT binding (p=0.08), except for a bilateral 33% reduction in 5-HTT binding in the mesial temporal cortex (p=0.0005). Smaller reductions in 5-HTT binding was found post hoc in prefrontal and occipital cortices, which was in contrast to the marked reduction in 5-HT$_{2A}$ binding of 28-39% throughout neocortex, even after correction for atrophy (PV correction). Since axonal 5-HTT sites show similar high-affinity binding properties as synaptic or perisynaptic 5-HTT [131], the cerebral binding of [^{11}C]DASB mainly represents the number of serotonergic axons projecting from the raphe nuclei [132]. Thus, the reduced [^{11}C]DASB binding in the mesial temporal lobes suggests a loss of projecting serotonergic axons to this region, whereas serotonergic projections to other neocortical regions and striatum are less affected. In post mortem studies of AD patients, similar reductions in 5-HTT have been demonstrated in temporal cortex [120], hippocampus and entorhinal cortex [116].

The small and non-significant 5-HTT reduction in striatum and most cortical regions appear to be in contrast to post mortem studies as well as to an *in vivo* PET study of combined [^{11}C]DASB and [^{18}F]FDG PET study of AD patients by Ouchi and coworkers [126]. This discrepancy is likely to be due to a combination of more severely affected patients in the study by Ouchi et al. in whom the mean dementia score (MMSE) was only 18 as compared to 24 in **study VII**. Furthermore, the lack of PV correction in the study by Ouchi et al. (2009) implies on the basis on the present work that the reported reduction in 5-HTT may stem from cerebral atrophy. Thus, the results from **study VII** suggests that loss of 5-HTT sites in AD occurs subsequent to the loss of cortical 5-HT$_{2A}$ receptors, although this conjecture would have to be tested in a PET study of longitudinal design.

The midbrain binding in dorsal raphe nucleus mainly represent the serotonergic cell bodies due to a large intracellular accumulation of 5-HTT in vesicles [133]. We found no group difference in 5-HTT binding in the dorsal raphe nucleus (p=0.70), which contrasts the histopathological studies in AD patients with pronounced loss of serotonin containing neurons or reduced 5-HT concentration in the raphe nuclei [114-117], as well as the *in vivo* imaging studie with reduced [^{11}C]DASB binding [126]. The difference between their data and ours could be due to differences in the approach for delineation of the raphe regions, however, part of the discrepancy is likely due to inclusion of patients at different stages of AD. If so, our observation suggests that the affection of serotonergic neurons is a late phenomenon in AD. The seemingly intact [^{11}C]DASB binding in the dorsal raphe of early AD patients is reminiscent of the cortical axotomy produced in pigs exposed to the serotonin toxin MDMA, in the absence of reduced number of serotonin neurons [134].

Tau pathology is prominent in the mesial temporal lobe early in the progression of AD, whereas beta-amyloid is more diffusely distributed in both mesial temporal lobe as well as in neocortical regions [91;135]. Correspondingly, post mortem stereology studies show loss of neurons in hippocampus in late AD patients [136] but no change of the number of neurons in preclinical AD [137] likewise in neocortex [96].

Table 5.
[^{18}F]altanserin (5-HT$_{2A}$) and [^{11}C]DASB (5-HTT) binding potentials in patients with AD compared to healthy control cases.

Region	Alzheimer patients		Healthy control cases		Diff.	Diff.	Volume of gray matter		
	5-HT$_{2A}$ BP_P	5-HTT BP_{ND}	5-HT$_{2A}$ BP_P	5-HTT BP_{ND}	5-HT$_{2A}$	5-HTT	AD cm^3	Controls cm^3	Diff.
men/women	8/3	7/4	6/5	6/4			8/4	6/5	
Striatum	0.46±0.44	1.69±0.46	0.56±0.35	1.84±0.25	-17%	-8.3%	10.1±2.1	10.1±0.8	0.3%
Prefrontal	2.11±1.20	0.50±0.08	2.97±0.50	0.57±0.06	-29%*	-12%*	24.4±5.3	24.5±2.6	-0.1%
Parietal	2.24±1.25	0.55±0.10	3.12±0.48	0.54±0.10	-28%*	+1.8%	47.6±9.1	51.2±4.3	-7.1%
Temporal	1.61±0.86	0.45±0.08	2.39±0.35	0.46±0.06	-33%*	-3.4%	66.7±12.1	68.6±7.8	-2.8%
Occipital	1.77±0.88	0.41±0.07	2.85±0.57	0.53±0.09	-38%**	-22%**	47.5±11.2	45.2±6.7	5.0%
Insula	0.82±0.50	0.76±0.18	1.36±0.35	0.78±0.11	-39%**	-3.2%	11.6±1.9	12.0±1.6	-3.7%
Anterior Cingulate	1.25±0.77	0.63±0.09	1.94±0.38	0.69±0.11	-36%*	-8.8%	5.59±1.0	5.61±0.81	-0.3%
Mesial Temporal	0.15±0.23	0.47±0.11	0.44±0.31	0.70±0.14	-66%*	-33%***	8.53±1.5	8.28±0.92	3.0%
"Non-specific binding"	2.11±0.93	4.24±0.64h	2.78±0.50	4.47±0.50h	-24%	-5.3%	-	-	-
Dorsal Raphe Nucleus	-	3.60±0.67	-	3.72±0.71	-	-3.1%	-	-	-

Non-specific binding is calculated as the ratio of radioactive concentration in cerebellum to plasma for [^{18}F]altanserin, and estimated as cerebellar area-under-curve (AUC) divided by injected dose per body mass for [^{11}C]DASB. The binding potential in dorsal raphe nucleus is an average of all included voxels (not only gray matter voxels) and no PV correction is applied, as the segmentation between gray and white matter in this region is unreliable. *p<0.05; **p<0.01; ***p<0.001.

In **study VII**, AD patients were predominantly in the mild stage, such that their tau pathology was most likely restricted to mesial temporal lobe, and it may thus be hypothesized that tau pathology and/or concurrent neurodegeneration in the mesial temporal cortex may be causative for the observed serotonergic axonal degeneration found in this region. Thus, a dying back degeneration of serotonergic axons in cortical structures with high tau load would explain the more profound reduction in [^{11}C]DASB binding in mesial temporal lobe, despite the absent changes in the [^{11}C]DASB binding in the raphe nuclei. Thus, the marked discrepancy between the global reduction in neocortical 5-HT$_{2A}$ receptor binding and the localized 5-HTT reduction may be a manifestation of dendritic degeneration evoked by diffuse β-amyloid polypeptide accumulation in neocortex [102], whereas the 5-HTT reduction is more indicative of specific degeneration of serotonergic axons in mesial temporal lobe structures. This hypothesis is in line with an experimental study, in which beta-amyloid infusion in mice caused a reduction in 5-HT$_{2A}$ receptor binding [138]. Furthermore, using autoradiography, Jensen and coworkers (Neurobiology Research Unit, Copenhagen) have studied 5-HT$_{2A}$ receptors and 5-HTT binding in a transgenic mouse model of AD (personal communication). In this model, increasing beta-amyloid load was related to a small, but significant reduction in cortical 5-HT$_{2A}$ receptor binding, whereas no significant reduction in 5-HTT was found. The mouse model differs from AD in humans with respect to the degree of neurodegeneration in mesial temporal lobe as the mice show no significant tau accumulation even in advanced stages of the disease. Thus, the findings of Jensen et al. support the notion that the 5-HTT reduction found in **study VII** is a later event and is related to loss or dysfunction of the terminal part of axons projecting to the mesial temporal lobe due to AD related neuropathology in these structures.

We found that the AD patients had significantly greater effects of PV correction on [^{18}F]altanserin binding estimates in the parietal, temporal, and prefrontal cortices for, and tendencies to higher effects of PV corrections on [^{11}C]DASB binding in striatum (p=0.07) and mesial temporal cortex (p=0.06). Further, significant correlations between gray matter volume and partial volume correction was found in insula, temporal, occipital cortices for [^{18}F]altanserin, and mesial temporal cortex for [^{11}C]DASB. Although no differences in gray matter volume were found (table 5), significant atrophy in some of the AD patients is likely to have been present, as cerebral atrophy structures other than gray matter will lead to enlarged sulci, thereby increasing the magnitude of the PV effect, e.g. white matter atrophy as noted in **study I**. Indeed, several regions showed more pronounced PV correction in AD patients as compared to control cases, and the correlations in several regions between gray matter volume and PV corrections support the use of the PV correction as a measure of overall atrophy.

The strength of **study VII** lies in the measurement of 5-HT$_{2A}$ and 5-HTT sites in the same individuals. Several methodological issues may affect the quantification of receptors *in vivo* by PET, but some of these are common to the two tracers studied, e.g., the PV correction is critically dependent upon correct segmentation of the MRI. Using, the same MRI segmentation for both tracers in each subject ensured the same PV correction for the two tracers. A limitation of **study VII** is due to small sample size and the use of a reference method for the calculation of 5-HTT binding potentials, as possible differences in non-displaceable binding may have biased our results. Although the AD patients and healthy control cases did not show any differences in the normalized [^{11}C]DASB concentration in cerebellum (area under curve), and the study by Ouchi and coworkers did not find group differences in V_{ND} (personal communication), care must be taken when comparing [^{18}F]altanserin BP_P, which is relative to plasma, and [^{11}C]DASB BP_{ND}, which is relative to non-displaceable binding in cerebellum.

Discussion and Perspectives

An inherent property of the stereological design is the mathematical unbiased estimation, which is based on mathematics and geometry. No assumptions of structure, form or size of the objects to be counted are necessary, and if sufficient repeated measurements are made, their true number would in principle be known. Caveats lie in the technical procedures of stereology. In particular, the major limitation of post mortem measurements is the occurrence of shrinkage artifacts, which can only be accounted for incompletely. In addition, possible structural changes during the antemortem period must be considered. Furthermore, the identification of structures is observer-dependent, which may call into question the accuracy of counting, and the observer must be blinded to the source of the sample.

In a stereologist objective, preferring numbers over densities and absolute values over ratios, the quantitative PET measurements fall short to the stereological standards of unbiased quantification. The outcome measure of PET examinations is often the binding potential, which is a ratio of f_{ND}*B_{max}/K_D in a particular brain region, thus proportional to the density of receptors (B_{max}). The binding parameter is frequently estimated by normalizing to the cerebellar concentration, thus unaccounted changes in numerous biological or technical parameters will possibly bias the result (see table 6).

Measuring the actual B_{max} instead of a binding potential would remove a substantial part of the assumptions. However, to achieve individual estimates in subjects at least three PET scans with a range of specific activities are necessary. The amount of radioactivity injected and the possible pharmaceutical effects from the ligand when tracer doses are not used, limit this procedure to animals for some ligands, although there is a considerable literature on the two-point estimates of the B_{max} of dopamine D_2 receptors in living human brain.

Applying stereological methods to PET is intriguing and stereological methods have indeed been applied to MRI analysis [139]. However, this approach is not directly transferable to PET, because PET studies reveal continuous distributions rather than discrete images of objects within a volume. Instead, the optimization of PET measures is these days directed towards increased resolution of the PET scanners. The latest human PET, the High Resolution

Table 6

Possible biases	How to account for this
B_{max} is the receptor concentration, i.e. a density	It is the measure of interest. Tissue volumes can be reported separately
f_{ND}, the fraction of free tracer in tissue	Cannot be measured *in vivo,* and not be sufficiently accounted for
K_D of the ligand (the inverse affinity)	*In vitro* examinations can probably rule out differences between groups or regions
V_{ND}, the non-displaceable binding in cerebellum	Can be measured with arterial input in conjunction with displacement studies to verify absence of a specific binding component
The tissue composition could change with a biased segmentation of the MRI into gray and white matter, whereby the PV correction would change	The possible effects of this are not known, and gray-white matter boundaries are not perfectly defined in MRI. Mixing is possible.
Enlargement of sulci leading to increased PV effect	The PV correction should correct for this
Too low specific activity leading to occupancy by unlabelled ligand	Can be measured in a separate study with multiple injections of a range of specific activities, or as in study V: population-based
Too low chemical purity leading to substances binding at other sites	This is controlled
The volume of the reference volume, e.g. the cortical gray matter could decline with a concomitant decrease in the total number of binding sites, such that no change in the density would be observed	The volumes can be measured, although biases in the measurements are possible
Technical properties of the scanner and the well counter	Regular cross calibration of scanners and well counters is mandatory
Numerous technical challenges in the MRI acquisition due to inhomogenity and non-uniformity of the magnetic field	Post processing of the MRI should correct for this
Partial volume effects in the MRI	Probably negligible relative to the resolution in PET

Research Tomograph (HRRT) (figure 3) has a theoretical resolution of a few millimeters. Although this resolution cannot be fully exploited due to technical issues and to the upper limit for injected dose, the improved resolution mitigates against PV effect for brain structures on the scale of the thickness of cortex, for example. Furthermore, numerous post-processing algorithms and reconstruction methods are continuously being developed, which achieve quantitatively more correct images with higher resolution in both MRI and PET.

A major concern in volumetric studies lies in the difference between post mortem volume estimates and MRI based methods for age-related changes in gray and white matter. In a cross-over study with domestic pigs, there were no significant differences between quantitative MRI *in vivo* and post mortem volume estimation using the Cavalieri applied to brain blocks [140]; done properly, the two methods should yield identical values. The vagaries of MRI volumetry are likely to depend on the chosen method of segmentation, and the definition of bounderies. In a study of human aging between 20 and 80 years, gray matter declined from 53% of intracranial volume to 43%, while white matter volume declined only slightly [97]. A peak in white matter volume should apparently appear around 60 years of age [53]. On the other hand, an interactive segmentation of the MRI in which the operator manually designated three tissue types (gray, white and cerebrospinal fluid), showed a normal age related gray matter reduction of 14% and a white matter reductions of 27% from 30 to 90 years of age [67], which is very close to the corresponding declines of 13% and 28% from 20 to 90 years, as reported from post mortem studies [4]. However, when employing SPM2 and the MNI template for segmentation, as in **study IV-VII**, most studies report large gray matter reductions and no significant white matter changes, e.g. [141]. In **study VI**, we found no white matter changes and significant gray matter reductions of 2-3% over two years of healthy aging in several cortical regions, which is clearly not in line with an overall reduction of 13-14% from 30-90 years. Even were there an accelerated loss in the interval from 60 to 90 years to 2% per two years, would predict a lifelong reduction of more than 26% in gray matter.

Possible biases in the segmentation will directly influence PET measures due to the gray matter masking of included voxels and the PV correction. Thus, optimization of the segmentation of the MRI is warranted and shall be implemented for future studies. With respect to this issue, results of **studies VI** and **VII**, could be biased due to the use SPM2 segmentation for elderly individuals. However, the conclusions of **study VI** are based on paired observations, with the calculation of variability between scans, thus a biased MRI segmentation would have been the same for both PET examinations. The conclusions of **study VII** are based on the comparison of 5-HT_{2A} and 5-HTT measures, both of which will be equally influenced by biased MRI segmentation, such that the conclusions of **study VI** and **VII** should be robust.

In summary, several quantitative methods of neuronal communication have been evaluated. The stereological methods allow for in principle unbiased quantitation of number, length, surfaces, and volumes among other quantities of biological interest. There was a post mortem finding of 45% reduction of total length of white matter myelinated fibers with age from 20 to 80 years of age (**study I**). There emerged no difference between schizophrenic patients (**study II**) or AD patients (**study III**) as compared to age-matched control cases.

Quantitative PET recordings rely on kinetic models based on a number of assumptions noted above, but allowing for *in vivo* measures of molecules at nanomolar concentrations. We validated the use of [^{11}C]SB207145, a novel tracer for quantitative PET imaging of 5-HT_4 receptors, and reported that reference-based methods (**study IV**) are applicable, although bias in the parameter estimation must be expected in high binding regions, and consistently high specific activity is necessary to avoid occupancy by unlabeled tracer (**study V**). However, we exploited the range of specific activities to obtain a population-based estimate of absolute receptor concentration, which proved to correlate with *in vitro* measures. A five-fold difference in B_{max} was found, which cannot readily be explained. No

change in 5-HT_{2A}-receptor binding was found during two-year follow-up study in elderly subjects, which indicates a stable serotonin system in elderly (**study VI**). The application of PV correction diminished the reliability of BP_P estimates, but allowed for the distinction between differences in atrophy and receptor binding. Furthermore, we found a relative preservation of serotonergic neurons and projections in patients with early AD, in contrast to the marked loss of post-synaptic 5-HT_{2A} receptors (**study VII**). These findings speak against a primary dysfunction of the serotonin system.

In conclusion, quantitative measures of neuronal communication were evaluated with the endpoint consisting of estimates of total length of myelinated nerve fibers post mortem material, whereas pre- and post-synaptic measures of serotonergic pathways were measured *in vivo*. In the post mortem study, the total length of myelinated nerve fibers was reproducibly estimated using mathematical unbiased methods in a material from 36 individuals. The finding of massive age-related reduction contributes to the understanding of white matter age effects, knowledge that could not necessarily have been achieved by MRI diffusion tensor imaging. The surprising lack of changes in myelinated fibers in schizophrenia and AD is an important contribution to the continuing search for the neuropathological basis of these devastating diseases.

The radioligand [^{11}C]SB207145 is going to be used at several sites for research and drug occupancy studies. The present validation of methods is a prerequisite for the studies. Findings draw attention to the focus on high specific activity, given the high sensitivity of outcome measures to occupancy by unlabeled ligand. This has increased the accuracy of the measuring and future studies exploiting the occupancy issue and the impact of AD on the 5-HT_4 receptors are ongoing.

Efforts to improve quantitation of serotonin marker through PV correction revealed that correction decreased inter-subject variation. This is a novel finding with importance for planning of new studies, and the requirements for group size. Our finding of preservation of serotonergic projections in AD, as distinct from declining serotonin receptor levels, contradicts earlier *post mortem* and *in vivo* findings in late Alzheimer's disease. Studying the early stages of the disease, as was done in **study VII**, is more likely to reflect the primary pathological changes, and the preserved serotonergic projections support the prevailing hypothesis of accumulating β-amyloid as a causal factor for degenerative changes. Further, the preserved serotonergic fibers support the use of SSRI as pharmacological treatment of neuropsychiatric symptoms in AD.

REFERENCES

1. Willis W: The Nervous System and Its Components; in Berne R, Levy M (eds): Physiology. St. Louis, Mosby Year Book, 1993,pp. 93-108.
2. Fields RD: Oligodendrocytes changing the rules: action potentials in glia and oligodendrocytes controlling action potentials. Neuroscientist. 2008;14:540-543.
3. Nadasdy Z: Spike sequences and their consequences. J Physiol Paris. 2000;94:505-524.
4. Pakkenberg B, Gundersen HJ: Neocortical neuron number in humans: effect of sex and age. J Comp Neurol. 1997;384:312-320.
5. Pelvig DP, Pakkenberg H, Stark AK, Pakkenberg B: Neocortical glial cell numbers in human brains. Neurobiol Aging. 2008;29:1754-1762.
6. Tang Y, Nyengaard JR, De Groot DM, Gundersen HJ: Total regional and global number of synapses in the human brain neocortex. Synapse. 2001;41:258-273.
7. Andersen BB, Gundersen HJ, Pakkenberg B: Aging of the human cerebellum: a stereological study. J Comp Neurol. 2003;466:356-365.
8. Gray JA, Roth BL: Paradoxical trafficking and regulation of 5-HT(2A) receptors by agonists and antagonists. Brain Res Bull. 2001;56:441-451.
9. Takano A, Arakawa R, Hayashi M, Takahashi H, Ito H, Suhara T: Relationship Between Neuroticism Personality Trait and Serotonin Transporter Binding. Biol Psychiatry. 2007;62:588-592.
10. Frokjaer VG, Mortensen EL, Nielsen FA et al: Frontolimbic Serotonin 2A Receptor Binding in Healthy Subjects Is Associated with Personality Risk Factors for Affective Disorder. Biol Psychiatry. 2008;63:569-576.
11. Varnas K, Halldin C, Pike VW, Hall H: Distribution of 5-HT4 receptors in the postmortem human brain--an autoradiographic study using [125I]SB 207710. Eur Neuropsychopharmacol. 2003;13:228-234.
12. Mohler EG, Shacham S, Noiman S et al: VRX-03011, a novel 5-HT4 agonist, enhances memory and hippocampal acetylcholine efflux. Neuropharmacology. 2007;53:563-573.
13. Orsetti M, Dellarole A, Ferri S, Ghi P: Acquisition, retention, and recall of memory after injection of RS67333, a 5-HT(4) receptor agonist, into the nucleus basalis magnocellularis of the rat. Learn Mem. 2003;10:420-426.
14. Terry AV, Jr., Buccafusco JJ, Jackson WJ et al: Enhanced delayed matching performance in younger and older macaques administered the 5-HT4 receptor agonist, RS 17017. Psychopharmacology (Berl). 1998;135:407-415.
15. Bockaert J, Claeysen S, Compan V, Dumuis A: 5-HT4 receptors. Curr Drug Targets CNS Neurol Disord. 2004;3:39-51.
16. Porras G, Di Matteo V, De Deurwaerdere P, Esposito E, Spampinato U: Central serotonin4 receptors selectively regulate the impulse-dependent exocytosis of dopamine in the rat striatum: in vivo studies with morphine, amphetamine and cocaine. Neuropharmacology. 2002;43:1099-1109.
17. Cai X, Flores-Hernandez J, Feng J, Yan Z: Activity-dependent bidirectional regulation of GABA(A) receptor channels by the 5-HT(4) receptor-mediated signalling in rat prefrontal cortical pyramidal neurons. J Physiol. 2002;540:743-759.
18. Yamaguchi T, Suzuki M, Yamamoto M: Evidence for 5-HT4 receptor involvement in the enhancement of acetylcholine release by p-

chloroamphetamine in rat frontal cortex. Brain Res. 1997;772:95-101.
19. Cachard-Chastel M, Lezoualc'h F, Dewachter I et al: 5-HT4 receptor agonists increase sAPPalpha levels in the cortex and hippocampus of male C57BL/6j mice. Br J Pharmacol. 2007;150:883-892.
20. Turner PR, O'Connor K, Tate WP, Abraham WC: Roles of amyloid precursor protein and its fragments in regulating neural activity, plasticity and memory. Prog Neurobiol. 2003;70:1-32.
21. Robert SJ, Zugaza JL, Fischmeister R, Gardier AM, Lezoualc'h F: The human serotonin 5-HT4 receptor regulates secretion of non-amyloidogenic precursor protein. J Biol Chem. 2001;276:44881-44888.
22. Cho S, Hu Y: Activation of 5-HT4 receptors inhibits secretion of beta-amyloid peptides and increases neuronal survival. Exp Neurol. 2007;203:274-278.
23. Lai MK, Tsang SW, Francis PT et al: [3H]GR113808 binding to serotonin 5-HT(4) receptors in the postmortem neocortex of Alzheimer disease: a clinicopathological study. J Neural Transm. 2003;110:779-788.
24. Wong EH, Reynolds GP, Bonhaus DW, Hsu S, Eglen RM: Characterization of [3H]GR 113808 binding to 5-HT4 receptors in brain tissues from patients with neurodegenerative disorders. Behav Brain Res. 1996;73:249-252.
25. Innis RB, Cunningham VJ, Delforge J et al: Consensus nomenclature for in vivo imaging of reversibly binding radioligands. J Cereb Blood Flow Metab. 2007;27:1533-1539.
26. Gundersen HJ, Bendtsen TF, Korbo L et al: Some new, simple and efficient stereological methods and their use in pathological research and diagnosis. APMIS. 1988;96:379-394.
27. Nyengaard JR: Stereologic methods and their application in kidney research. J Am Soc Nephrol. 1999;10:1100-1123.
28. Gundersen H: Notes on the estimation of the numerical density of arbitrary profiles: The edge effect. J Microsc. 1977;111:219-223.
29. Gundersen H: Estimation of tubule or cylinder LV, SV and VV on thick sections. J Microsc. 1979;117:333-345.
30. Syvanen S, Blomquist G, Sprycha M et al: Duration and degree of cyclosporin induced P-glycoprotein inhibition in the rat blood-brain barrier can be studied with PET. Neuroimage. 2006;32:1134-1141.
31. Laruelle M, Slifstein M, Huang Y: Positron emission tomography: imaging and quantification of neurotransporter availability. Methods. 2002;27:287-299.
32. Hume SP, Myers R, Bloomfield PM et al: Quantitation of carbon-11-labeled raclopride in rat striatum using positron emission tomography. Synapse. 1992;12:47-54.
33. Slifstein M, Parsey RV, Laruelle M: Derivation of [(11)C]WAY-100635 binding parameters with reference tissue models: effect of violations of model assumptions. Nucl Med Biol. 2000;27:487-492.
34. Lammertsma AA, Hume SP: Simplified reference tissue model for PET receptor studies. Neuroimage. 1996;4:153-158.
35. Logan J, Fowler JS, Volkow ND et al: Graphical analysis of reversible radioligand binding from time-activity measurements applied to [N-11C-methyl]-(-)-cocaine PET studies in human subjects. J Cereb Blood Flow Metab. 1990;10:740-747.
36. Logan J, Fowler JS, Volkow ND, Wang GJ, Ding YS, Alexoff DL: Distribution volume ratios without blood sampling from graphical analysis of PET data. J Cereb Blood Flow Metab. 1996;16:834-840.
37. Ichise M, Liow JS, Lu JQ et al: Linearized reference tissue parametric imaging methods: application to [11C]DASB positron emission tomography studies of the serotonin transporter in human brain. J Cereb Blood Flow Metab. 2003;23:1096-1112.
38. Moller M, Jakobsen S, Gjedde A: Parametric and regional maps of free serotonin 5HT1A receptor sites in human brain as function of age in healthy humans. Neuropsychopharmacology. 2007;32:1707-1714.
39. Gunn RN, Gunn SR, Turkheimer FE, Aston JA, Cunningham VJ: Positron emission tomography compartmental models: a basis pursuit strategy for kinetic modeling. J Cereb Blood Flow Metab. 2002;22:1425-1439.
40. Gee AD, Martarello L, Passchier M et al: Synthesis and Evaluation of [^{11}C]SB207145 as the First *In Vivo* Serotonin 5-HT$_4$ Receptor Radioligand for PET Imaging in Man. Current Radiopharmaceuticals. 2008;1:110-114.
41. Wu Y, Carson RE: Noise reduction in the simplified reference tissue model for neuroreceptor functional imaging. J Cereb Blood Flow Metab. 2002;22:1440-1452.
42. Kornum BR, Lind NM, Gillings N, Marner L, Andersen F, Knudsen GM: Evaluation of the novel 5-HT(4) receptor PET ligand [(11)C]SB207145 in the Göttingen minipig. J Cereb Blood Flow Metab. 2009;29:186-196.
43. Pinborg LH, Adams KH, Svarer C et al: Quantification of 5-HT2A receptors in the human brain using [18F]altanserin-PET and the bolus/infusion approach. J Cereb Blood Flow Metab. 2003;23:985-996.
44. Svarer C, Madsen K, Hasselbalch SG et al: MR-based automatic delineation of volumes of interest in human brain PET images using probability maps. Neuroimage. 2005;24:969-979.
45. Abi-Dargham A, Simpson N, Kegeles L et al: PET studies of binding competition between endogenous dopamine and the D1 radiotracer [11C]NNC 756. Synapse. 1999;32:93-109.
46. Gunn RN, Lammertsma AA, Hume SP, Cunningham VJ: Parametric imaging of ligand-receptor binding in PET using a simplified reference region model. Neuroimage. 1997;6:279-287.

47. Hammers A, Asselin MC, Turkheimer FE et al: Balancing bias, reliability, noise properties and the need for parametric maps in quantitative ligand PET: [(11)C]diprenorphine test-retest data. Neuroimage. 2007;38:82-94.
48. Claeysen S, Sebben M, Becamel C et al: Pharmacological properties of 5-Hydroxytryptamine(4) receptor antagonists on constitutively active wild-type and mutated receptors. Mol Pharmacol. 2000;58:136-144.
49. Arakawa R, Ito H, Takano A et al: Dose-finding study of paliperidone ER based on striatal and extrastriatal dopamine D2 receptor occupancy in patients with schizophrenia. Psychopharmacology (Berl). 2008;197:229-235.
50. Reynolds GP, Mason SL, Meldrum A et al: 5-Hydroxytryptamine (5-HT)4 receptors in post mortem human brain tissue: distribution, pharmacology and effects of neurodegenerative diseases. Br J Pharmacol. 1995;114:993-998.
51. Holden JE, Jivan S, Ruth TJ, Doudet DJ: In vivo receptor assay with multiple ligand concentrations: an equilibrium approach. J Cereb Blood Flow Metab. 2002;22:1132-1141.
52. Ostergaard SD, Alstrup AK, Gramsbergen JB et al: MDMA-evoked changes in the binding of dopamine D(2) receptor ligands in striatum of rats with unilateral serotonin depletion. Synapse. 2009;64:70-82.
53. Westlye LT, Walhovd KB, Dale AM et al: Life-Span Changes of the Human Brain White Matter: Diffusion Tensor Imaging (DTI) and Volumetry. Cereb Cortex. 2009.
54. Highley JR, Esiri MM, McDonald B, Roberts HC, Walker MA, Crow TJ: The size and fiber composition of the anterior commissure with respect to gender and schizophrenia. Biol Psychiatry. 1999;45:1120-1127.
55. Meier-Ruge W, Ulrich J, Bruhlmann M, Meier E: Age-related white matter atrophy in the human brain. Ann N Y Acad Sci. 1992;673:260-9.:260-269.
56. Aboitiz F, Rodriguez E, Olivares R, Zaidel E: Age-related changes in fibre composition of the human corpus callosum: sex differences. Neuroreport. 1996;7:1761-1764.
57. Hildebrand C, Remahl S, Persson H, Bjartmar C: Myelinated nerve fibres in the CNS. Prog Neurobiol. 1993;40:319-384.
58. Tang Y, Nyengaard JR: A stereological method for estimating the total length and size of myelin fibers in human brain white matter. J Neurosci Methods. 1997;73:193-200.
59. Nyengaard JR, Gundersen H: The isector: a simple and direct method for generating isotropic, uniform random sections from small specimens. J Microsc. 1991;165:427-431.
60. Zhang W, Li C, Yang S et al: A stereological method for estimating the total length and size of myelinated fibers in rat cerebral cortex. J Neurosci Methods. 2008;172:21-26.
61. Tang Y, Nyengaard JR, Pakkenberg B, Gundersen HJ: Age-induced white matter changes in the human brain: a stereological investigation. Neurobiol Aging. 1997;18:609-615.
62. Christiansen P, Larsson HB, Thomsen C, Wieslander SB, Henriksen O: Age dependent white matter lesions and brain volume changes in healthy volunteers. Acta Radiol. 1994;35:117-122.
63. Barkhof F, Scheltens P: Imaging of white matter lesions. Cerebrovasc Dis. 2002;13 Suppl 2:21-30.:21-30.
64. Brun A, Englund E: A white matter disorder in dementia of the Alzheimer type: a pathoanatomical study. Ann Neurol. 1986;19:253-262.
65. Albert M: Neuropsychological and neurophysiological changes in healthy adult humans across the age range. Neurobiol Aging. 1993;14:623-625.
66. Guttmann CR, Jolesz FA, Kikinis R et al: White matter changes with normal aging. Neurology. 1998;50:972-978.
67. Jernigan TL, Archibald SL, Fennema-Notestine C et al: Effects of age on tissues and regions of the cerebrum and cerebellum. Neurobiol Aging. 2001;22:581-594.
68. Miller AK, Corsellis JA: Evidence for a secular increase in human brain weight during the past century. Ann Hum Biol. 1977;4:253-257.
69. Peters A, Sethares C, Luebke JI: Synapses are lost during aging in the primate prefrontal cortex. Neuroscience. 2008;152:970-981.
70. Peters A: The effects of normal aging on myelinated nerve fibers in monkey central nervous system. Front Neuroanat. 2009;3:11. Epub;%2009 Jul 6.:11.
71. Peters A: Age-related changes in oligodendrocytes in monkey cerebral cortex. J Comp Neurol. 1996;371:153-163.
72. Ludwin SK: The pathobiology of the oligodendrocyte. J Neuropathol Exp Neurol. 1997;56:111-124.
73. Kojima T, Matsushima E, Ohta K et al: Stability of exploratory eye movements as a marker of schizophrenia--a WHO multi-center study. World Health Organization. Schizophr Res. 2001;52:203-213.
74. Weinberger DR, Egan MF, Bertolino A et al: Prefrontal neurons and the genetics of schizophrenia. Biol Psychiatry. 2001;50:825-844.
75. Pakkenberg B, Scheel-Kruger J, Kristiansen LV: Schizophrenia; from structure to function with special focus on the mediodorsal thalamic prefrontal loop. Acta Psychiatr Scand. 2009;120:345-354.
76. Pakkenberg B: Total nerve cell number in neocortex in chronic schizophrenics and controls estimated using optical disectors. Biol Psychiatry. 1993;34:768-772.
77. Thune JJ, Uylings HB, Pakkenberg B: No deficit in total number of neurons in the prefrontal cortex in schizophrenics. J Psychiatr Res. 2001;35:15-21.
78. Pakkenberg B: Pronounced reduction of total neuron number in mediodorsal thalamic nucleus

and nucleus accumbens in schizophrenics. Arch Gen Psychiatry. 1990;47:1023-1028.
79. Dorph-Petersen KA, Pierri JN, Sun Z, Sampson AR, Lewis DA: Stereological analysis of the mediodorsal thalamic nucleus in schizophrenia: volume, neuron number, and cell types. J Comp Neurol. 2004;472:449-462.
80. Buchanan RW, Vladar K, Barta PE, Pearlson GD: Structural evaluation of the prefrontal cortex in schizophrenia. Am J Psychiatry. 1998;155:1049-1055.
81. Wible CG, Anderson J, Shenton ME et al: Prefrontal cortex, negative symptoms, and schizophrenia: an MRI study. Psychiatry Res. 2001;108:65-78.
82. Hulshoff Pol HE, Schnack HG, Bertens MG et al: Volume changes in gray matter in patients with schizophrenia. Am J Psychiatry. 2002;159:244-250.
83. Wible CG, Shenton ME, Hokama H et al: Prefrontal cortex and schizophrenia. A quantitative magnetic resonance imaging study. Arch Gen Psychiatry. 1995;52:279-288.
84. Baare WF, Hulshoff Pol HE, Hijman R, Mali WP, Viergever MA, Kahn RS: Volumetric analysis of frontal lobe regions in schizophrenia: relation to cognitive function and symptomatology. Biol Psychiatry. 1999;45:1597-1605.
85. Sanfilipo M, Lafargue T, Rusinek H et al: Volumetric measure of the frontal and temporal lobe regions in schizophrenia: relationship to negative symptoms. Arch Gen Psychiatry. 2000;57:471-480.
86. Hirayasu Y, Tanaka S, Shenton ME et al: Prefrontal gray matter volume reduction in first episode schizophrenia. Cereb Cortex. 2001;11:374-381.
87. Kyriakopoulos M, Bargiotas T, Barker GJ, Frangou S: Diffusion tensor imaging in schizophrenia. Eur Psychiatry. 2008;23:255-273.
88. Chance SA, Highley JR, Esiri MM, Crow TJ: Fiber content of the fornix in schizophrenia: lack of evidence for a primary limbic encephalopathy. Am J Psychiatry. 1999;156:1720-1724.
89. Groenewegen HJ, Wright CI, Uylings HB: The anatomical relationships of the prefrontal cortex with limbic structures and the basal ganglia. J Psychopharmacol. 1997;11:99-106.
90. Fuster JM: The prefrontal cortex--an update: time is of the essence. Neuron. 2001;30:319-333.
91. Braak H, Braak E: Neuropathological stageing of Alzheimer-related changes. Acta Neuropathol. 1991;82:239-259.
92. Launer LJ: Epidemiology of white matter lesions. Top Magn Reson Imaging. 2004;15:365-367.
93. Salat DH, Tuch DS, van der Kouwe AJ et al: White matter pathology isolates the hippocampal formation in Alzheimer's disease. Neurobiol Aging. 2010;31:244-256.
94. Gurol ME, Irizarry MC, Smith EE et al: Plasma beta-amyloid and white matter lesions in AD, MCI, and cerebral amyloid angiopathy. Neurology. 2006;66:23-29.
95. Pelvig DP, Pakkenberg H, Regeur L, Oster S, Pakkenberg B: Neocortical glial cell numbers in Alzheimer's disease. A stereological study. Dement Geriatr Cogn Disord. 2003;16:212-219.
96. Regeur L, Jensen GB, Pakkenberg H, Evans SM, Pakkenberg B: No global neocortical nerve cell loss in brains from patients with senile dementia of Alzheimer's type. Neurobiol Aging. 1994;15:347-352.
97. Fotenos AF, Snyder AZ, Girton LE, Morris JC, Buckner RL: Normative estimates of cross-sectional and longitudinal brain volume decline in aging and AD. Neurology. 2005;64:1032-1039.
98. Hubbard BM, Anderson JM: A quantitative study of cerebral atrophy in old age and senile dementia. J Neurol Sci. 1981;50:135-145.
99. Li S, Pu F, Shi F, Xie S, Wang Y, Jiang T: Regional white matter decreases in Alzheimer's disease using optimized voxel-based morphometry. Acta Radiol. 2008;49:84-90.
100. Berg L, McKeel DW, Jr., Miller JP et al: Clinicopathologic studies in cognitively healthy aging and Alzheimer's disease: relation of histologic markers to dementia severity, age, sex, and apolipoprotein E genotype. Arch Neurol. 1998;55:326-335.
101. Berg KA, Harvey JA, Spampinato U, Clarke WP: Physiological relevance of constitutive activity of 5-HT2A and 5-HT2C receptors. Trends Pharmacol Sci. 2005;26:625-630.
102. Hasselbalch SG, Madsen K, Svarer C et al: Reduced 5-HT2A receptor binding in patients with mild cognitive impairment. Neurobiol Aging. 2008;29:1830-1838.
103. Meltzer CC, Price JC, Mathis CA et al: PET imaging of serotonin type 2A receptors in late-life neuropsychiatric disorders. Am J Psychiatry. 1999;156:1871-1878.
104. Adams KH, Pinborg LH, Svarer C et al: A database of [(18)F]-altanserin binding to 5-HT(2A) receptors in normal volunteers: normative data and relationship to physiological and demographic variables. Neuroimage. 2004;21:1105-1113.
105. Meltzer CC, Smith G, DeKosky ST et al: Serotonin in aging, late-life depression, and Alzheimer's disease: the emerging role of functional imaging. Neuropsychopharmacology. 1998;18:407-430.
106. Haugbol S, Pinborg LH, Arfan HM et al: Reproducibility of 5-HT(2A) receptor measurements and sample size estimations with [(18)F]altanserin PET using a bolus/infusion approach. Eur J Nucl Med Mol Imaging. 2007;34:910-915.
107. Meltzer CC, Leal JP, Mayberg HS, Wagner HN, Jr., Frost JJ: Correction of PET data for partial volume effects in human cerebral cortex by MR imaging. J Comput Assist Tomogr. 1990;14:561-570.
108. Müller-Gartner HW, Links JM, Prince JL et al: Measurement of radiotracer concentration in brain gray matter using positron emission tomography: MRI-based correction for partial volume effects. J Cereb Blood Flow Metab. 1992;12:571-583.

109. Kalbitzer J, Svarer C, Frokjaer VG et al: A probabilistic approach to delineating functional brain regions. J Nucl Med Technol. 2009;37:91-95.
110. Smith GS, Price JC, Lopresti BJ et al: Test-retest variability of serotonin 5-HT2A receptor binding measured with positron emission tomography and [18F]altanserin in the human brain. Synapse. 1998;30:380-392.
111. Elmenhorst D, Meyer PT, Matusch A, Winz OH, Zilles K, Bauer A: Test-retest stability of cerebral A(1) adenosine receptor quantification using [(18)F]CPFPX and PET. Eur J Nucl Med Mol Imaging. 2007;34:1061-1070.
112. Neeb H, Zilles K, Shah NJ: Fully-automated detection of cerebral water content changes: study of age- and gender-related H2O patterns with quantitative MRI. Neuroimage. 2006;29:910-922.
113. Pinborg LH, Arfan H, Haugbol S et al: The 5-HT2A receptor binding pattern in the human brain is strongly genetically determined. Neuroimage. 2008;40:1175-1180.
114. Aletrino MA, Vogels OJ, Van Domburg PH, Ten Donkelaar HJ: Cell loss in the nucleus raphes dorsalis in Alzheimer's disease. Neurobiol Aging. 1992;13:461-468.
115. Halliday GM, McCann HL, Pamphlett R et al: Brain stem serotonin-synthesizing neurons in Alzheimer's disease: a clinicopathological correlation. Acta Neuropathol. 1992;84:638-650.
116. Tejani-Butt SM, Yang J, Pawlyk AC: Altered serotonin transporter sites in Alzheimer's disease raphe and hippocampus. Neuroreport. 1995;6:1207-1210.
117. Hendricksen M, Thomas AJ, Ferrier IN, Ince P, O'Brien JT: Neuropathological study of the dorsal raphe nuclei in late-life depression and Alzheimer's disease with and without depression. Am J Psychiatry. 2004;161:1096-1102.
118. Tsang SW, Lai MK, Francis PT et al: Serotonin transporters are preserved in the neocortex of anxious Alzheimer's disease patients. Neuroreport. 2003;14:1297-1300.
119. Thomas AJ, Hendriksen M, Piggott M et al: A study of the serotonin transporter in the prefrontal cortex in late-life depression and Alzheimer's disease with and without depression. Neuropathol Appl Neurobiol. 2006;32:296-303.
120. Chen CP, Alder JT, Bowen DM et al: Presynaptic serotonergic markers in community-acquired cases of Alzheimer's disease: correlations with depression and neuroleptic medication. J Neurochem. 1996;66:1592-1598.
121. Lai MK, Tsang SW, Francis PT et al: Reduced serotonin 5-HT1A receptor binding in the temporal cortex correlates with aggressive behavior in Alzheimer disease. Brain Res. 2003;974:82-87.
122. Bowen DM, Najlerahim A, Procter AW, Francis PT, Murphy E: Circumscribed changes of the cerebral cortex in neuropsychiatric disorders of later life. Proc Natl Acad Sci U S A. 1989;86:9504-9508.
123. Cheng AV, Ferrier IN, Morris CM et al: Cortical serotonin-S2 receptor binding in Lewy body dementia, Alzheimer's and Parkinson's diseases. J Neurol Sci. 1991;106:50-55.
124. Lai MK, Tsang SW, Alder JT et al: Loss of serotonin 5-HT2A receptors in the postmortem temporal cortex correlates with rate of cognitive decline in Alzheimer's disease. Psychopharmacology (Berl). 2005;179:673-677.
125. Lorke DE, Lu G, Cho E, Yew DT: Serotonin 5-HT2A and 5-HT6 receptors in the prefrontal cortex of Alzheimer and normal aging patients. BMC Neurosci. 2006;7:36.:36.
126. Ouchi Y, Yoshikawa E, Futatsubashi M, Yagi S, Ueki T, Nakamura K: Altered brain serotonin transporter and associated glucose metabolism in Alzheimer disease. J Nucl Med. 2009;50:1260-1266.
127. Kepe V, Barrio JR, Huang SC et al: Serotonin 1A receptors in the living brain of Alzheimer's disease patients. Proc Natl Acad Sci U S A. 2006;103:702-707.
128. Lanctot KL, Hussey DF, Herrmann N et al: A positron emission tomography study of 5-hydroxytryptamine-1A receptors in Alzheimer disease. Am J Geriatr Psychiatry. 2007;15:888-898.
129. Truchot L, Costes N, Zimmer L et al: A distinct [18F]MPPF PET profile in amnestic mild cognitive impairment compared to mild Alzheimer's disease. Neuroimage. 2008;40:1251-1256.
130. Blin J, Baron JC, Dubois B et al: Loss of brain 5-HT2 receptors in Alzheimer's disease. In vivo assessment with positron emission tomography and [18F]setoperone. Brain. 1993;116:497-510.
131. Zhou FC, Tao-Cheng JH, Segu L, Patel T, Wang Y: Serotonin transporters are located on the axons beyond the synaptic junctions: anatomical and functional evidence. Brain Res. 1998;805:241-254.
132. Nielsen K, Brask D, Knudsen GM, Aznar S: Immunodetection of the serotonin transporter protein is a more valid marker for serotonergic fibers than serotonin. Synapse. 2006;59:270-276.
133. Bunin MA, Wightman RM: Quantitative evaluation of 5-hydroxytryptamine (serotonin) neuronal release and uptake: an investigation of extrasynaptic transmission. J Neurosci. 1998;18:4854-4860.
134. Cumming P, Moller M, Benda K et al: A PET study of effects of chronic 3,4-methylenedioxymethamphetamine (MDMA, "ecstasy") on serotonin markers in Gottingen minipig brain. Synapse. 2007;61:478-487.
135. Price JL, Morris JC: Tangles and plaques in nondemented aging and "preclinical" Alzheimer's disease. Ann Neurol. 1999;45:358-368.
136. West MJ, Coleman PD, Flood DG, Troncoso JC: Differences in the pattern of hippocampal neuronal loss in normal ageing and Alzheimer's disease. Lancet. 1994;344:769-772.
137. West MJ, Kawas CH, Stewart WF, Rudow GL, Troncoso JC: Hippocampal neurons in pre-clinical Alzheimer's disease. Neurobiol Aging. 2004;25:1205-1212.

138. Christensen R, Marcussen AB, Wortwein G, Knudsen GM, Aznar S: Abeta(1-42) injection causes memory impairment, lowered cortical and serum BDNF levels, and decreased hippocampal 5-HT(2A) levels. Exp Neurol. 2008;210:164-171.
139. Roberts N, Puddephat MJ, McNulty V: The benefit of stereology for quantitative radiology. Br J Radiol. 2000;73:679-697.
140. Jelsing J, Rostrup E, Markenroth K et al: Assessment of in vivo MR imaging compared to physical sections in vitro--a quantitative study of brain volumes using stereology. Neuroimage. 2005;26:57-65.
141. Smith CD, Chebrolu H, Wekstein DR, Schmitt FA, Markesbery WR: Age and gender effects on human brain anatomy: a voxel-based morphometric study in healthy elderly. Neurobiol Aging. 2007;28:1075-1087.

ABBREVIATIONS AND NOMENCLATURE

- 1TC, 2TC, 3TC models – one, two, and three tissue compartment models
- 2D – two dimensional
- 3D – three dimensional
- 5-HT = 5-Hydroxy-tryptophan, serotonin
- 5-HT_{1A}, 5-HT_{2A}, 5-HT_4 receptors – subgroups of serotonin receptors
- 5-HTT – serotonin transporter
- AD – Alzheimer's disease
- Affinity – the attraction of the ligand to the receptor
- Akaike Information Criterion – a measure of goodness-of-fit used as a tool for model selection. The score is based on the error in the fit and the number of parameters in the model
- Axon – the nerve fiber is a long slender projection of a nerve cell that conducts electrical impulses away from the cell body
- B_{max} – the receptor concentration
- Bias – a statistical term for a systematic error in or confounder behind the measures. This is in contrast to noise, which should vary randomly
- BP_{ND} = binding potential relative to non-displaceable binding
- BP_P = binding potential relative to plasma concentration
- C_{ND} =concentration of ligand in reference tissue
- C_P = Plasma concentration of ligand
- C_S = concentration of specifically bound ligand
- C_{FT} = concentration of ligand in free tissue water
- Convolution: designated $\otimes$ – a mathematical operation on two functions. It is defined as the integral of the product of the two functions of changing quantity
- Coregistration – aligning the PET and the MRI image to each other
- DSM III – Diagnostic and statistical manual of mental disorders
- DTI – diffusion tensor imaging – MRI method that enables the measurement of restricted diffusion of water in tissue
- ED_{50} – An effective dose in pharmacology is the amount of drug that produces a therapeutic response in 50% of the people taking it. In PET used as the dose at which 50% of receptors are occupied
- f_P or f_{ND} – the free fraction (non-protein bound) of free ligand in plasma or in tissue
- K_1 and K_1' – Unidirectional blood brain clearance (mL cm^{-3} min^{-1}) for tissue and reference tissue
- k_2, k_3 and k_4 – fraction rate constants (min^{-1}) describing the flux of tracer into and between tissue compartments
- k_2' – k_2 for the reference region
- HPLC = high performance liquid chromatography
- *ICC* – Intraclass correlation coefficient, which denotes reliability of a measure by relating the variance between and within subjects in a test-retest setting. -1 denotes no reliability and 1 denotes maximum reliability
- K_D – the dissociation constant, which is the inverse of the affinity
- Ligand – the radiolabeled molecule used for imaging, synonymous with tracer
- Logan plot – a linearized method for calculating distribution volumes or binding potentials
- MRI – magnetic resonance imaging, used here for obtaining structural information about the brain
- MRTM – multilinear reference tissue model
- MRTM2 – multilinear reference tissue model with fixed k_2', i.e. washout rate of the reference tissue
- Myelin – the fatty cell membrane from oligodendrocytes ensheathing the axon, whereby the speed of conduction is increased
- Oligodendrocyte – a type of glia cell forming the myelin sheaths around axons.
- One or two tissue compartment model – a kinetic model described by one or two tissue compartments in the brain, i.e. non specific and specific binding
- P-glycoprotein – an efflux transporter in the blood-brain-barrier that limits the influx of potential harmful substances to the brain
- PET – positron emission tomography
- PV – partial volume, the spill-in and spill-out between the brain tissues in a PET scan due to the limited resolution
- $R_1=(K_1/K_1')$ – relative tracer delivery
- Reference region – PET nomenclature for a volume or region, which is biologically similar

to the region of interest, but is devoid of specific binding. Often cerebellum is used
- Reference volume – stereological nomenclature for the total volume of the tissue under study
- SRTM – simplified reference tissue model
- T2-weighted MRI – an MRI sequence that is especially sensitive to water content
- V_{ND} = Non-displaceable distribution volume
- V_T = Total distribution volume, consisting of bound and free tracer